Author responses to referee comments, 2018-02-15

We thank the anonymous referee once again for kindly providing the constructive critique. We provide the answers to the comments below.

Comment 1: please include a comparison to CO2 data from the eddy tower

Response 1: We have added a figure showing the CO2 flux from the eddy tower and the flux predicted by the model, and we added a short description of this to the text.

Changes to MS 1: Added Fig. 10 and its caption on p. 50, and a short section in the text, p. 17 l. 3-6.

Comment 2: about CH4:CO2 ratio: Why is that now different for exudates and bulk organic matter. You are using 0.4 for bulk OM and 0.7 for exudates. I cannot see a scientific explanation for this huge difference. Please, discuss this difference in teh MS secition discussion and explore what are the consequences for a future application of the model.

Response 2: The anaerobic respiration is modeled according to two separate processes that are assumed to be different, and therefore there are two different parameters controlling the processes. However, it is true that the difference ends up being quite large after the model calibration. We have added a paragraph noting this discrepancy, and suggesting that in future studies that parameter could also be added to the set of optimized parameters. We also mention that due to the posterior structure this has less effect on the fluxes than it might look based on looking at the difference between the two numbers, but that the balance of the processes could be slightly affected.

Changes to MS 2: Added paragraph on p. 18, l. 15-27.

Calibrating the sqHIMMELI v1.0 wetland methane emission model with hierarchical modeling and adaptive MCMC

Jouni Susiluoto[1,3,4], Maarit Raivonen[2], Leif Backman[1,2], Marko Laine[1], Jarmo Makela[1,4], Olli Peltola[2], Timo Vesala[2,5], and Tuula Aalto[1]

[1]Climate research, Finnish Meteorological Institute, P.O. Box 503, 00101 Helsinki, Finland
[2]Institute for Atmospheric and Earth System Research/Physics, Faculty of Science, University of Helsinki, Finland
[3]Lappeenranta University of Technology, School of Science, Finland
[4]University of Helsinki, Department of Mathematics and Statistics, Finland
[5]Institute for Atmospheric and Earth System Research/Forest Sciences, Faculty of Agriculture and Forestry, University of Helsinki, Finland

Correspondence to: jouni.susiluoto@fmi.fi

Abstract. Estimating methane (CH_4) emissions from natural wetlands is complex and the estimates contain large uncertainties. The models used for the task are typically heavily parametrized and the parameter values are not well known. In this study we perform a Bayesian model calibration for a new wetland CH_4 emission model to improve quality of the predictions and to understand the limitations of such models.

The detailed process model that we analyze contains descriptions for CH_4 production from anaerobic respiration, CH_4 oxidation, and gas transportation by diffusion, ebullition, and the aerenchyma cells of vascular plants. The processes are controlled by several tunable parameters. We use a hierarchical statistical model to describe the parameters and obtain the posterior distributions of the parameters and uncertainties in the processes with adaptive MCMC, importance resampling and timeseries analysis techniques. For the estimation, the analysis utilizes measurement data from the Siikaneva flux measurement site in Southern Finland.

The uncertainties related to the parameters and the modeled processes are described quantitatively. At the process level, the flux measurement data are able to constrain the CH_4 production processes, methane oxidation and the different gas transport processes. The posterior covariance structures explain how the parameters and the processes are related. Additionally, the flux and flux component uncertainties are analyzed both at the annual and daily levels. The parameter posterior densities obtained provide information regarding importance of the different processes, which is also useful for development of wetland methane emission models other than sqHIMMELI.

The hierarchical modeling allows us to assess the effects of some of the parameters on an annual basis. The results of the calibration and the cross validation suggest that the early spring net primary production could be used to predict parameters affecting the annual methane production.

Even though the calibration is specific to the Siikaneva site, the hierarchical modeling approach is well suited for larger scale studies and the results of the estimation pave way for a regional or global scale Bayesian calibration of wetland emission models.

1 Introduction

Methane is the third most important gas in the atmosphere in terms of its capacity to warm the climate, after water vapor and carbon dioxide, currently with the radiative forcing of 0.97 Wm^{-2} (IPCC, 2013). This is a sizable part of the total effect of well-mixed greenhouse gases, which is approximately 3.0 Wm^{-2}. According to IPCC (2013), the amount of CH_4 in the atmosphere has risen to its highest level in at least the last 800000 years due to human activity, and based on ice core measurements, also its growth rate is presently very likely at its highest level in the last 22000 years.

The sources of CH_4 are both anthropogenic and natural. In years 2003-2012, 60% of the global emissions were anthropogenic (range 50-65 %) and about one third came from natural wetlands. The most important source of uncertainty in the global methane budget is attributable to emissions from wetlands and other inland waters. Combining top-down and bottom-up estimates, natural wetland emissions range from 127 to 227 Tg CH_4 yr^{-1} (Saunois et al., 2016). Anthropogenic sources include rice paddies, landfills, enteric fermentation and manure, incomplete combustion of hydrocarbons, and natural gas leaks (Ciais et al., 2013).

The methane from wetlands is produced by prokaryotic archaea under anaerobic conditions. The main sink for atmospheric CH_4 is its oxidation in troposphere by OH and the average lifetime of a CH_4 molecule in the atmosphere is 9.1 ± 0.9 years (Prather et al., 2012; IPCC, 2013).

The wetlands in the boreal zone are a significant contributor to the total CH_4 emissions from wetlands (Kirschke et al., 2013), and for this reason the CH_4 emissions from them have been intensively studied, also with models, during the past years (Wania et al., 2010; Kaiser et al., 2016; Petrescu et al., 2015). However, major discrepancies between predictions from those models remain (Melton et al., 2013; Bohn et al., 2015).

The need for improved wetland methane emission modeling is amplified by the fact that although annual mean precipitation is projected to increase in the boreal zone (Ruosteenoja et al., 2016), changes in the frequency and duration of severe drought may follow an alternate path (Lehtonen et al., 2014), manifesting the need to study wetland responses to extreme events.

Changes to hydrological conditions such as draining or recurring low water table depth can alter the balance of greenhouse gas emissions (Frolking et al., 2011; Petrescu et al., 2015). Modeling and calibrating for such exceptional events can be difficult, as was found for instance by Mäkelä et al. (2016).

The HelsinkI Model of MEthane buiLd-up and emIssion for peatlands (HIMMELI) is a relatively full-featured wetland/peatland CH_4 emission model and it is described in detail in Raivonen et al. (2017). The model contains process descriptions for CH_4 production from anaerobic respiration, O_2 consumption and CO_2 production from oxic respiration, and gas transport processes via diffusion, ebullition, and plant transport. Modeling the concentrations of CH_4, O_2, and CO_2 in the peat column is explicitly included. The peat column depth can be set at any desired value, and the water table movement determines the part of the peat column that is favorable for CH_4 production. The version of HIMMELI in this work has additional processes, described in Sec. 3.1, and the modified model is referred to as sqHIMMELI (square root HIMMELI), as it contains a description of CH_4 production from root exudates. The sqHIMMELI model is geared towards site-level studies, whereas HIMMELI is more suited for integration directly as a component in e.g. land surface schemes.

Even well constructed computer models describing environmental processes accumulate error at many levels (Sanso et al., 2007). The sources include time- and space discretization, compromises in model physics and biochemistry descriptions due to computational constraints, insufficient information about the initial states of the model, and numerical errors, along with parametrization-induced inaccuracies of the subgridsize processes. This leads to a need to calibrate and optimize models, as the physical variables do not necessarily exactly correspond to the model variables and hence the model parameters cannot often be directly measured. Of course any physically insightful interpretation of calibration results makes sense only for a well-constructed physical model.

Several current CH_4 models include the important physical processes controlling both CH_4 production and transport in the peat column (Kaiser et al., 2016; Lai, 2009b; Müller et al., 2015; Grant and Roulet, 2002). The modeled peat column depth affects the total modeled CH_4 emission from the peatlands and it is directly included in some models (Lai, 2009b; Walter and Heimann, 2000). These models are in general highly sensitive to changes in the values of the parameters (van Huissteden et al., 2009). However, even though algorithmic parameter optimization has been done in some studies, the stress is often on parameter efficiencies (van Huissteden et al., 2009), or optimal values (Müller et al., 2015), and hence the full uncertainty of the values of parameters in these models is not well understood.

Methane models typically use measured values from field campaigns and parameters estimated from those studies where applicable (Lai, 2009b; Walter and Heimann, 2000; Tang et al., 2010; Riley et al., 2011), and, when needed, include extra tuning parameters for processes (Walter and Heimann, 2000). This is a practical and much used route as information regarding all of the needed parameters is not available at all sites (van Huissteden et al., 2009; Walter and Heimann, 2000). Wide variability can be expected from some parameters, such as those controlling CH_4 oxidation (Segers, 1998). Emissions from different areas of the same wetland can also vary, due to microtopography and differences between how fast the peat decomposes in different areas (Lai, 2009a; Cresto Aleina et al., 2016), making straightforward parameter value assignment difficult.

Due to these uncertainties, values of parameters vary widely from research to research. For instance for the Q_{10}-value controlling the temperature dependence of CH_4 production, Walter and Heimann (2000) use the value 6, handpicking it from the interval of 1.7-16, whereas van Huissteden et al. (2009) use a range of 3-8, and Müller et al. (2015) constrain the value between 1 and 10, with the default value of 1.33 and eventually optimizing it to the value of 1 for two of the three optimizations presented. For other parameters, such as those controlling diffusion rates in peat, the situation is similar.

Calibration done for the models is usually quite basic. Wania et al. (2010) tune their model by running it with parameters from a parameter grid, containing only three values for each of the 7 parameters tested, and Riley et al. (2011) follow a similar procedure for the wetland CH_4 model component, CLM4Me, of the Community Land Model. Such sensitivity studies obviously are not able to find out how a model is able to perform at its best. Müller et al. (2015) have further optimized the CLM4Me model using an emulator combined with a simple minimization algorithm, with respect to several different sites, which are bound to have quite different physical characteristics, and are yielding optimal values often at the borders of the prescribed allowed area of variation. In a sensitivity analysis of the PEATLAND-VU model, a derivative of the Walter-Heimann model, van Huissteden et al. (2009) look at the efficiencies of the different parameters, but do not elaborate on other qualities of the posterior.

Using hierarchical modeling to estimate annually varying parameters is sensible, since the flux measurement site has both properties that change from year to year (e.g. small changes in vegetation, plant roots, and microbe populations) and properties that are more permanent (e.g. peat quality and plant species). With fixed parameter values for all years, the model sometimes does not accurately and appropriately describe the observations. On the other hand, with different parameters for all the years, the parameters are easily overfitted, meaning that while the resulting model fits the data well, it does not accurately predict future fluxes (Gelman et al., 2013). Hierarchical modeling provides a solution for these problems.

In the present study, the sqHIMMELI model is calibrated using adaptive Markov chain Monte Carlo (MCMC) and importance resampling techniques to evaluate a hierarchical statistical model for the model parameters. The calibration is done for the boreal Siikaneva site. This study complements the work in Raivonen et al. (2017) in describing the effects of various parameters on the processes and fluxes, and analyzing what kinds of configurations best describe the studied boreal wetland.

Merely optimizing model parameters may lead to misleading results due to the presence of several local minima in the objective function, as for example Müller et al. (2015) reported in a study where they used a surrogate model to calibrate the parameters of the CH_4 model component of the Community Land Model. This multi-modality can be accommodated for by using MCMC techniques. Utilizing MCMC methods for optimizing environmental models and studying their uncertainties is not new (Laine, 2008; Ricciuto et al., 2008; Hararuk et al., 2014), but to our knowledge they have not been used for wetland CH_4 model parameter estimation before. Moreover, the research that the authors are aware of does not investigate the interannual variability of parameters, as is done in this study.

The main objective of this work is to analyze the capabilities and limitations of a modern featureful wetland CH_4 model by looking into the shape of the posterior parameter distributions, parameter correlations, and the roles, identifiabilities, interdependencies, and interconnections of the parameters and the processes they control. As a part of this work, knowledge about how the methane and carbon dioxide flux data are able constrain the parameters and processes, is obtained.

2 Siikaneva wetland flux measurement site and model input data

Methane and carbon dioxide flux measurements were needed for estimating the model parameters, and for that purpose observational data from the Siikaneva peatland flux measurement site in southern Finland (61°50'N, 24°12'E) were used. The site is a boreal oligotrophic fen with a peat depth of up to four meters.

Measurement of ecosystem scale gas fluxes started in 2005, and in this work eddy covariance (EC) CH_4 and CO_2 flux measurements from years 2005 to 2014 were used. In the current application of the EC method, the gas fluxes were calculated from the wind speed and direction, and CH_4 and CO_2 concentration information. All these variables were sampled with 10 Hz and fluxes were calculated over 30-min averaging time in order capture the whole spectrum of turbulent exchange. During the measurement period several different instruments were used for methane concentration measurements: Campbell TGA-100 (2005-2007 and 04/2010-08/2010), Los Gatos RMT-200 (01/2008-02/2014), Picarro G1301-f (04/2010-10/2011) and Los Gatos FGGA (2014). Carbon dioxide concentrations were measured throughout the period with a LI-7000 manufactured by Licor Inc. The wind velocity vector was analyzed by a USA-1 acoustic anemometer by METEK (Rinne et al., 2007). All the

EC-data were post-processed in a consistent manner using an in-house software EddyUH (Mammarella et al., 2016). Flux data were screened for instrumental problems and for insufficient turbulent mixing. Due to instrument problems, data from 2009 was not available.

For this study daily means of CH_4 fluxes were calculated from the screened data that contained gaps. This is a viable approach, since CH_4 fluxes do not show a diel pattern at this site (Rinne et al., 2007). However, before calculating the daily values of net ecosystem exchange of CO_2, standard gap-filling methods for peatland CO_2 fluxes were applied (Aurela et al., 2001, 2007). In short, the gap-filling algorithm estimated the CO_2 flux dependency on photosynthetic photon flux density, air temperature and water table position and the algorithm was used to fill periods when CO_2 fluxes were missing. See more details in (Aurela et al., 2001, 2007) about the gap-filling procedure. After gap-filling the daily means of CO_2 fluxes were calculated and used in this study.

For using this carbon dioxide data with the costfunction, the CO_2-flux produced by sqHIMMELI was matched with the sum of net ecosystem exchange and the net primary production of all plants. We assumed that the share of aerenchymatous plants is 70% of the total NPP. The fact that the net primary production is not a measured but modeled quantity (see below) introduces some uncertainty into the CO_2 flux against which the model is calibrated.

The required inputs for sqHIMMELI are daily soil temperatures, water table depths (WTD), net primary production (NPP), and leaf area indexes (LAI). The soil temperature profile for the grid used was generated by interpolating from measurement data between the measurement depths (-5 cm, -10 cm, -20 cm, -35 cm and -50 cm) and assuming that at -3 meters and below the temperature is a constant +7 °C. This was the mean temperature of all the years at -50 cm depth. The WTD data used was available as measurement data, and where data was missing, it was gap-filled by repeating the previous measured value. Net primary production cannot be measured in a direct way, and hence values obtained from a regression model were used. The methodology is explained in Appendix E and still further in Raivonen et al. (2017). Similarly for LAI, a simple model was used for obtaining the input. The details are, again, given in Appendix E. A summary of the data used is given in Table 1.

3 The sqHIMMELI model

The HIMMELI (HelsinkI Model of MEthane buiLd-up and emIssion for peatlands) model (Raivonen et al., 2017) is a detailed model for estimating CH_4 emissions from wetlands. It was developed at the University of Helsinki in collaboration with the Finnish Meteorological Institute and the Max Planck Institute for Meteorology in Hamburg. The model is designed to be used as a submodel in different modeling environments, such as regional and global biosphere models. It contains processes describing the production of CH_4 and CO_2 including anaerobic production of CO_2, the loss of CH_4 and O_2, and transport of CH_4, O_2, and CO_2 between the soil and the atmosphere. The CH_4 transport can take place by diffusion in peat (in water and in the air), by ebullition (transport by bubble formation), and by diffusion in the porous aerenchyma tissues in vascular plants. The model is driven with peat temperature, WTD and LAI of the aerenchymatous plants. The process descriptions are mainly adopted from previous wetland CH_4 models such as Arah and Stephen (1998), Wania et al. (2010) and Tang et al. (2010). The

version of the model used here differs slightly from that presented in (Raivonen et al., 2017), and is therefore called with the different name of sqHIMMELI to avoid confusion.

The model simulates the processes in a discretized peat column. The number and thickness of the peat layers can be varied, but in this work six 10 cm layers is used, similarly to e.g. Kaiser et al. (2016), with one thicker bottom layer under these, so that the total modeled peat column depth is 85% of the maximum observed 4 m depth of the wetland, i.e. 3.4 m. The water table divides the column into water-filled and air-filled parts, and CH_4 is produced only in the inundated anoxic layers. In the present configuration, the NPP-related CH_4 production is allocated into the layers according to the vertical distribution of the root mass, described in Sect. 3.2. The internal time resolution of the model is dynamically adjusted depending on the model state, and the output interval is set to one day.

At present, the model does not contain descriptions for processes related to snow pack or ice such as diffusion through snow, or release of accumulated gas bubbles under ice in spring time as described by e.g. Mastepanov et al. (2013) and Sriskantharajah et al. (2012).

HIMMELI itself, as presented in Raivonen et al. (2017), does not simulate carbon uptake (photosynthesis) or peat carbon pools but instead it takes as input the rate of anoxic respiration. The differences between HIMMELI and sqHIMMELI are described below in Sec. 3.1 and 3.2 and in Sec. 3.5.3.

For each modeled process in sqHIMMELI, there are parameters regulating the process, affecting the concentrations of CH_4, O_2 and CO_2 in the peat column, and the wetland methane emissions. The equations describing the physics relevant to the optimized parameters are listed in section 3.4. Other relevant model equations are listed in Sec. 3.5.

3.1 Root exudates and peat decomposition

Methanogens prefer recently assimilated fresh carbon as their energy source, for instance the root exudates of vascular plants (Joabsson and Christensen, 2001). A connection between ecosystem productivity and CH_4 emission has been observed in several wetland studies (Bellisario et al., 1999; Whiting and Chanton, 1993). However, anoxic decomposition of litter and older peat also produces CH_4 (Hornibrook et al., 1997). Many models form CH_4 substrates by extracting directly a fraction of the net primary production (van Huissteden et al., 2009; Wania et al., 2010), and some rely on heterotrophic peat respiration only (Riley et al., 2011). In sqHIMMELI both primary production and anaerobic peat decomposition were included.

The modified sqHIMMELI model contains an exudate pool description, from which it produces methane (Eq. 3 and 15). The exudate pool itself is described by Eq. 4, detailing how the modeled NPP turns into root exudates. Effectively, a fraction of NPP determined by the parameter ζ_{exu} (-) produces root exudates, which are then distributed as anaerobic respiration according to the root distribution into the peat column at the rate determined by the model parameter τ_{exu} (s). The part ending up under the water table produces CH_4 and CO_2, depending on the oxygen content of the water, and above the water table the exudates are respired into CO_2.

The second source of anaerobic respiration, the anaerobic peat decomposition, is modeled in sqHIMMELI with a simple Q_{10}-model adopted from Schuldt et al. (2013). The peat under the water table is prescribed a turnover time, based on which anaerobic respiration and CH_4 are produced according to Eq. 5 and 16.

3.2 Root distributions

The sqHIMMELI model differs from HIMMELI in the details regarding the root distribution model. Compared to measurement data of root distributions of aerenchymatous sedges from Saarinen (1996), the original root distribution $\pi(z)$, adopted from Wania et al. (2010) and described by

$$\pi(z) \propto \exp(-z/\lambda_{\mathrm{root}}), \tag{1}$$

does not describe the distribution of roots well. Here z is depth, and λ_{root} is a parameter describing the steepness of the decaying exponential curve. This formula is replaced with

$$\pi(z) \propto C_0 \exp\left[-\frac{(z-z_0)^2}{\lambda_{\mathrm{root}}^2}\right] + C_1. \tag{2}$$

With the Gaussian shape, the new root density decreases faster with depth. Without this change, the optimization process calibrates the model to have very high root masses below 50 cm underground. The other difference between the models is that in the original model there are vanishingly few roots below the depth of one meter, but according to Saarinen (1996), sedge roots can reach to as low as 2.3 m under the surface. The term C_1 in Eq. 2 was added to remedy this.

Before starting the optimization, the parameters C_0, C_1, and z_0 were fitted to data from Saarinen (1996), resulting in values of $C_0 = 215$, $C_1 = 6$, and $z_0 = 0.105$. The different root distributions are shown in Fig. 1.

3.3 Peat depth

Methane is produced from anaerobic peat decomposition at all peat depths in the sqHIMMELI model, and its transport and oxidation affect the modeled CH_4 emission. The homogeneous model description of the peat column is highly idealized, as in reality the peat column varies from place to place with respect to CH_4 production rate, production depth, and gas transport. We model the peat column to be 3.4 meters deep, which is 85% of the maximum observed depth of the Siikaneva wetland. Small uncertainty in the value of the parameter is acceptable since the parameter τ_{cato}, which regulates the rate of peat decomposition into CH_4, can partly compensate for this uncertainty.

3.4 Parameter descriptions for sqHIMMELI

The parameters for the optimization were chosen to constrain the processes most important for the CH_4 emission. Of the optimized parameters, all but ζ_{exu} (-) and Q_{10} (-) are the same for all years. However, ζ_{exu} and Q_{10} change year to year to reflect the changes in the relative CH_4 input to the system from peat decomposition and NPP-based production. This will allow to analyze the year to year changes in relative importances of the production pathways. The setup is natural, as for example Bergman et al. (2000) report the Q_{10}-values changing from measurement date to another, even within a single year. As the values reported for minerotrophic lawn in Bergman et al. (2000) indicate that they may vary quite irregularly within a growing season, the modeling performed here does not take intra-annual variations into account and concentrates on the year to year variation. Possible mechanisms for the parameter variations include variations in substrate supply and desiccation stress and are

discussed in e.g. Davidson et al. (2006). Table 2 shows the parameters that are used in the equations below but not optimized in this work, along with their values and explanations of why they were left out. The list of calibrated parameters along with their physical meanings is presented below.

CH_4 production-related parameters

1. τ_{exu} (s): Controls the decay rate of exudates, ν, from the root exudate pool P_{exu},
$$\nu = \frac{P_{\mathrm{exu}}}{\tau_{\mathrm{exu}}}. \tag{3}$$

2. ζ_{exu} (-): Fraction of NPP carbon that goes to the root exudate pool.
$$\frac{\mathrm{d}P_{\mathrm{exu}}}{\mathrm{d}t} = -\nu + \psi_t \zeta_{\mathrm{exu}}, \tag{4}$$
where ψ_t is the rate of NPP at time t, P_{exu} is size of the root exudate pool, and ν was given by Eq. 3.

3. τ_{cato} (y): Controls the base rate of peat decomposition into CH_4 in Eq. 5.

4. Q_{10} (-): Controls the temperature dependence of the rate of peat decomposition into CH_4 in anaerobic conditions via factor k_{cato}, given by the equation
$$k_{\mathrm{cato}} = Q_{10}^{\frac{(T-273.15)}{10}} / \tau_{\mathrm{cato}}. \tag{5}$$

5. $f_{CH_4}^{\mathrm{exu}}$ (-): Fraction controlling the methane production from anaerobic respiration of root exudates in Eq. 15.
$$R_{CH_4}^{\mathrm{exu}}(z) = \frac{f_{CH_4}^{\mathrm{exu}}}{\mathrm{d}z} \nu \frac{\pi(z)}{1 + \eta C_{O_2}(z)}.$$
Here $\pi(z)$ is the root distribution from Eq. 2, and ν is described in Eq. 3. The equation is discussed in Sec. 3.5.2.

Oxidation and respiration parameters

6. V_{R0} (mol m^{-3} s^{-1}): Respiration parameter controlling the rate of heterotrophic respiration, which consumes O_2 and produces CO_2. This affects the rate of temperature dependent heterotrophic respiration, $V_R(z)$, given by
$$V_R(z) = V_{R0} \exp\left(\frac{\Delta E_R}{R} (\frac{1}{283} - \frac{1}{T(z)}) \right). \tag{6}$$
Here ΔE_R (J mol^{-1}) is a parameter affecting the temperature dependence of the heterotrophic respiration, R is the universal gas constant, and $T(z)$ is temperature at depth z.

7. ΔE_R (J mol^{-1}): Described above in context of Eq. 6.

8. V_{O0} (mol m^{-3} s^{-1}): CH_4 oxidation parameter controlling the potential rate of CH_4 oxidation V_O:
$$V_O(z) = V_{O0} \exp\left(\frac{\Delta E_{\mathrm{oxid}}}{R} (\frac{1}{283} - \frac{1}{T(z)}) \right). \tag{7}$$

9. ΔE_{oxid}: Described in Eq. 7, affecting temperature response of CH_4 oxidation.

Gas transport-related parameters

10. λ_{root} (m): Controls how the root mass is distributed. See Eq. 2.

11. ρ (m^2 kg^{-1}): Root-ending area per root biomass, affecting root conductance, see Eq. 8.

12. τ (m m^{-1}): Root tortuousity parameter affecting the root conductance K_R. A tortuousity of 1 means that the roots are not decreasing the conductance via their curvedness. The equation for the conductance is

$$K_R(z) = \frac{D_{\mathrm{air}} m \rho \pi(z)}{\tau z}, \tag{8}$$

where $\pi(z)$ is the root mass density as a function of depth, over which the sum of the density is one, and m is the total root mass per square meter, set to be proportional to LAI.

13. $f_{D,a}$ (-): Fraction of the diffusion rate in air-filled peat divided by the diffusion rate in free air. The parameter affects the diffusion and the plant transport fluxes in the model: the higher this parameter is, the more there is diffusion as it takes a shorter time for the CH_4 to exit the peat reducing the possibility of oxidation and increasing the concentration gradient driving diffusion. The equation is

$$D_{\mathrm{air}} = f_{D,a} D_{\mathrm{air}}^{273} \left(\frac{T}{298} \right)^{1.82}, \tag{9}$$

where D_{air} is the diffusion rate in air-filled peat, D_{air}^{273} is the diffusion base rate at $273K$, and T is the temperature. The effect on plant transport comes via Eq. 8 .

14. $f_{D,w}$ (-): Same as above, but in water. The equation describing the peat-water diffusion rate is

$$D_{\mathrm{water}} = f_{D,w} D_{\mathrm{water}}^{298} \frac{T}{298}, \tag{10}$$

where the terms are analogous to the ones in Eq. 9.

3.5 The sqHIMMELI model equations

The version of HIMMELI presented here describes processes for CH_4 production and transport. It differs from the version presented in Raivonen et al. (2017) in that the model presented there does not contain the processes for anaerobic respiration but rather take it as input, the idea being that such input would be available when using HIMMELI as a part of a larger model. Hence the equations presented in Sec. 3.5.2 are specific to the version used in this study. The other difference between the models is the difference between the root distributions described in Sec. 3.2.

3.5.1 Governing equations

The gas concentrations of CH_4, carbon dioxide and oxygen in the peat column are governed by the equations

$$T_X(t,z) = Q_X^{\mathrm{diff}} + Q_X^{\mathrm{plant}} + Q_X^{\mathrm{ebu}} \tag{11}$$

$$\frac{\partial[\mathrm{CH_4}]}{\partial t}(t,z) = -T_{CH_4} + R_{CH_4}^{\mathrm{exu}} + R_{CH_4}^{\mathrm{peat}} - R_{CH_4}^{\mathrm{oxid}} \tag{12}$$

$$\frac{\partial[\mathrm{O_2}]}{\partial t}(t,z) = -T_{O_2} - R_{\mathrm{aerob}}^{\mathrm{peat}} - R_{CO_2}^{\mathrm{exu}} - 2R_{CH_4}^{\mathrm{oxid}} \tag{13}$$

$$\frac{\partial[\mathrm{CO_2}]}{\partial t}(t,z) = -T_{CO_2} + R_{CO_2}^{\mathrm{exu}} + R_{CO_2}^{\mathrm{peat}} + R_{CH_4}^{\mathrm{oxid}} + R_{\mathrm{aerob}}^{\mathrm{peat}}, \tag{14}$$

where $T_X(t,z)$ describes transport of gas X containing the diffusion, ebullition, and plant transport components, and R stands for production or consumption. The different terms in the equations are described below.

3.5.2 Anaerobic respiration producing CH_4

The equations presented in this section are specific to the version of HIMMELI used in this study. The version in Raivonen et al. (2017) takes the rate of anaerobic decomposition of carbon as input and does not treat the different sources of that carbon separately.

The carbon for methane production in this model version comes from two sources: root exudates and anaerobic peat decomposition. The methane production from anaerobic respiration of that carbon is given by the terms $R_{CH_4}^{\mathrm{exu}}$ and $R_{CH_4}^{\mathrm{peat}}$ described by:

$$R_{CH_4}^{\mathrm{exu}}(z) = \frac{f_{CH_4}^{\mathrm{exu}}}{\mathrm{d}z}\nu\frac{\pi(z)}{1+\eta C_{O_2}(z)} \tag{15}$$

$$R_{CH_4}^{\mathrm{peat}}(z) = k_{\mathrm{cato}}(z) g_{CH_4}^{Q_{10}} \frac{\rho_{\mathrm{cato}} f_{C_{\mathrm{cato}}}}{M_C}, \tag{16}$$

where in Eq. 15 ν is the decay rate of root exudates from Eq. 3, η is an oxygen inhibition parameter, $C_{O_2}(z)$ is the oxygen concentration at depth z, and $\pi(z)$ is the normalized proportion of the total anaerobic root mass, also at depth z, given in an unnormalized form in Eq. 2. The decay rate of root exudates does not depend on the peat column thickness. The parameter $f_{CH_4}^{\mathrm{exu}}$ (-) determines what fraction of root exudates in anaerobic conditions will turn into CH_4. Equation 15 is only used below the water table. The anoxic peat decomposition described by Eq. 16 depends on the amount of peat and its temperature, among others. The factor $g_m^{Q_{10}}$ (-) is the proportion of the anaerobic peat decomposition process producing CH_4, ρ_{cato} is the peat density in the catotelm, $f_{C_{\mathrm{cato}}}$ is the fraction of carbon in catotelm peat, and M_C is the molar mass of carbon. The parameter $k_{\mathrm{cato}} = Q_{10}^{\frac{(T-273.15)}{10}}/\tau_{\mathrm{cato}}$ is described in Eq. 5, and is zero above water table.

The equations for CO_2 are similar:

$$R_{CO_2}^{\mathrm{exu}}(z) = \nu\pi(z) - R_{CH_4}^{\mathrm{exu}}(z) \tag{17}$$

$$R_{CO_2}^{\mathrm{peat}}(z) = (1 - g_{CH_4}^{Q_{10}}) k_{\mathrm{cato}}(z) \frac{\rho_{\mathrm{cato}} f_{C_{\mathrm{cato}}}}{M_C}, \tag{18}$$

and the meanings of the symbols are analogous to the ones in equations for CH_4.

3.5.3 Peat respiration and methane oxidation

Peat respiration (aerobic respiration) is described with an equation of the Michaelis-Menten form

$$R^{\mathrm{peat}}_{\mathrm{aerob}}(z) = V_R(z)\frac{\alpha C^w_{O_2}(z)}{K_R + C^w_{O_2}(z)}, \tag{19}$$

where $C^w_{O_2}$ is the oxygen concentration in water. Above the water table we assume a water phase that is in equilibrium with the gas phase, i.e. $C^w_{O_2} = \alpha C^a_{O_2}$. The parameter α is a dimensionless Henry solubility constant for oxygen. Parameter K_R is the Michaelis-Menten constant of the process, and $V_R(z)$ is given by Eq. 6. Methane oxidation is controlled by dual-substrate Michaelis-Menten kinetics,

$$R^{\mathrm{oxid}}_{CH_4}(z) = V_O(z)\frac{C^w_{O_2}(z)}{K_{O_2} + C^w_{O_2}(z)}\frac{C^w_{CH_4}(z)}{K_{CH_4} + C^w_{CH_4}(z)}, \tag{20}$$

and here the terms are analogous to those in Eq. 19, except for that the term $V_O(z)$ is described by Eq. 7.

3.5.4 CH_4 transport

The transport term $T_X(t,z)$ in Eq. 11 consist of the following terms:

$$Q^{\mathrm{diff}}_X = D^X_{\mathrm{medium}}\frac{\partial}{\partial z}C^{\mathrm{medium}}_X \tag{21}$$

$$Q^{\mathrm{plant}}_X(z) = \frac{\rho\pi(z)D^X_{\mathrm{air}}}{\tau^2}\frac{LAI}{SLA}\frac{C_x(t,z) - C^{\mathrm{atm}}_X}{z} \tag{22}$$

$$Q^{\mathrm{ebu}}_X(z) = -k\sigma\frac{pp_{i,X}}{RT}\frac{\sum_i pp_i(z) - (P_{\mathrm{atm}} + P_{\mathrm{hyd}}(z))}{\sum_i pp_i(z)}. \tag{23}$$

The first of these is the diffusion, where the diffusion coefficients D are given by Eq. 9 and 10, and "medium" refers to either air or water. The second equation is for plant transport, with ρ ($\mathrm{m^2\ kg^{-1}}$) and τ ($\mathrm{m\ m^{-1}}$) described in context of Eq. 8, $\pi(z)$ is the normalized root distribution mentioned above, and C^{atm}_X refers to the atmospheric partial pressure of gas X. LAI stands for the leaf area index, given as input, and SLA is the specific leaf area. The third equation is the ebullition component of the gas transport, where pp_i refers to the partial pressure of different gases indexed with i, R is the universal gas constant, k is an ebullition rate constant, and σ is the peat porosity. The parameters P_{atm} and $P_{\mathrm{hyd}}(z)$ refer to the atmospheric pressure and hydrostatic pressure at depth z, respectively.

4 Model calibration

The model calibration consists of several steps, but can be summarized as first estimating the posterior with MCMC and then based on those results, re-calibrating the objective function and using this new formulation for importance resampling. Importance resampling is typically used for obtaining posterior distributions from minor changes to the objective function descriptions (Gelman et al., 2013). This is also its purpose here.

In more detail, first, a posterior estimate was drawn running 500000 iterations of sqHIMMELI simulations with the Adaptive Metropolis Markov chain Monte Carlo algorithm with a Laplace-distributed error description and a first order autoregressive

model, AR(1), for the residuals. Second, for defining the more refined costfunction for importance resampling the optimal order for an autoregressive moving average (ARMA) timeseries model for the model residuals was identified from the maximum a posteriori estimate by minimizing the Akaike and Bayesian Information Criteria with respect to the model order. The third step was drawing a random sample of size fifty from the posterior estimate obtained with MCMC, with which the error model parameters α and γ, described in conjunction to the details of the error model in Eq. A3, were calibrated by minimizing the Kullback-Leibler divergence (Kullback and Leibler, 1951) with respect to the standard Laplace distribution for the methane and carbon dioxide separately. The median of the obtained parameters was chosen for the second costfunction used in the importance resampling. Fourth, a random sample of size 10000 was drawn from the MCMC posterior and importance resampling was performed by drawing a subsample of size 1500 utilizing weights calculated with the new costfunction values obtained from the above mentioned error model calibration as described by e.g. Gelman et al. (2013).

The need for the importance resampling arises from that the error model transformed methane and carbon dioxide residuals emerging from the maximum a posteriori and posterior mean estimates from the calibration with the AR(1) model are not fully independent and identically distributed. The recalibration of the error model, and resampling from the simulated posterior using importance resampling, remedies this problem, as can be seen in the residual histogram and autocorrelation functions in Fig. 2.

4.1 Hierarchical description of parameters

In order to be able to assess the annual parameter and CH_4 transport pathway changes, a hierarchical description for two of the parameters was used. These parameters were Q_{10} (-) controlling the temperature dependence of the peat decomposition rate, and ζ_{exu} (-), regulating the production of root exudates from NPP.

The *hyperparameters* are the means and variances defining the Gaussian priors of the hierarchical parameters Q_{10} (-) and ζ_{exu} (-). They were updated using fixed Gaussian *hyperpriors* with Gibbs sampling. The sampling distribution depends on the current values of the hyperparameters. The role of the hyperprior is to constrain the distribution from which the hyperparameters are sampled.

Technically, a *Metropolis-within-Gibbs*-method (Gelman et al., 2013) for sampling the hierarchical parameters, non-hierarchical parameters, and the hyperparameters was used, presented briefly in Appendix C. The model parameters (i.e. everything except the hyperparameters) were sampled with the Adaptive Metropolis (AM) MCMC algorithm (Haario et al., 2001), which uses a Gaussian proposal distribution, whose covariance matrix is adapted as the chain evolves, and over time the acceptance rate gets closer to an optimal value, which is 0.23 for Gaussian targets in large dimensions (Roberts et al., 1997). If the algorithm proposes values outside the hard parameter limits listed in table 3, the model will not be evaluated and the value is rejected.

Our empirical data for the hierarchical model were the nine years from 2006 to 2014, meaning that for each of these years there were corresponding ζ_{exu} (-) and Q_{10} (-) parameters in the optimization. The model was spun up for each annual flux estimation in order to have a realistic column of gas concentrations available. For this reason, the previous year was always also simulated, and for the likelihood only the residuals from the latter year were included in the calculations. Therefore year

2005 did not contribute directly to the values of the objective function. The different years were run in parallel to save execution time.

4.2 Objective functions for MCMC and importance resampling

As in many practical uncertainty quantification applications, a major part of the parameter estimation problem is the proper definition of the objective function. For MCMC it is defined here based on *a priori* information about the measurement uncertainties, based on information from the model residuals, and based on additional prior information. For the importance resampling we modify the error model for the CO_2 and CH_4 residual components of the objective function based on an analysis of the MCMC results.

4.2.1 Model residuals and error model

The form of the objective function is the same for both MCMC and importance resampling. The first two components of the objective function contain the contributions from the modeled differences to the daily CH_4 and CO_2 flux measurements. In the MCMC objective function it is assumed that the daily flux estimate uncertainties are dependent on approximately a fraction α of the flux measurement (Richardson et al., 2006) and some constant error, γ (e.g. measurement device precision). The model error is expected to follow a similar form, and hence α and γ contain the contributions from both the model and measurement errors. For importance resampling the description is the same except for that a 14-day running mean of the interannual variability is used for α. These parameters are set independently for both CH_4 and CO_2.

When determining the parameters γ and α, the resulting residuals end up being autocorrelated. Therefore they are treated as such with the AR(1)-model for MCMC and with the ARMA(2,1)-model for the importance resampling, described e.g. in Chatfield (1989).

Since the primary interest is in the methane fluxes, the carbon dioxide residuals are scaled down to a fifth in the importance resampling costfunction, which is enough to guide the parameter values since several years of CO_2 flux data are used. Furthermore, as the model does not contain descriptions for the effects of snow and ice on the fluxes, the fit cannot be expected to be very good in the winter months. Therefore we further only consider 20% of the contribution of the residuals in the winter season from December to February. The obtained residuals, denoted by the ϵ-terms in the objective function, Eq. 24, are treated as Laplace-distributed. The flux observation errors are reported to follow a distribution of this type, rather than a Gaussian distribution (Richardson et al., 2006). The error model is explained in more detail in Appendix A.

4.2.2 Prior information

The parameters affecting the CH_4 production of the wetland model are not known well, but despite this, not setting any prior distributions on parameters can lead to nonphysical parameter values in the posterior distribution.

The parameter priors are set to zero outside prescribed bounds. Within these bounds, the parameters are assigned Gaussian priors, with the exception of one parameter whose prior is set to be flat. The prior values are based on both literature and expert knowledge and the information regarding the parameter values is summarized in Table 3.

4.2.3 The objective function

The *objective function* for the parameter optimization, $J(\boldsymbol{\theta})$, is the negative logarithm of the value of the unnormalized posterior probability density function at $\boldsymbol{\theta}$. It combines our statistical knowledge of the flux observations and parameter priors presented in Sec. 4.2.1 – 4.2.2, and is given by:

$$J(\boldsymbol{\theta}) = -\log\left(p(\boldsymbol{\theta}|\boldsymbol{y})\right) = \sum_{i=1}^{N_{\mathrm{obs}}^{\mathrm{CH_4}}} |\epsilon_i^{\mathrm{CH_4}}| + \sum_{j=1}^{N_{\mathrm{obs}}^{\mathrm{CO_2}}} |\epsilon_j^{\mathrm{CO_2}}| + \frac{1}{2}\sum_{k=1}^{N_{par}} \frac{(\theta_k - \mu_k)^2}{\sigma_k^2} \tag{24}$$

Here $\epsilon_t^{\cdot}$ are the AR(1) or ARMA(2,1)-transformed Laplace-distributed residuals, and the last term is the prior contribution, where θ_k is the proposed parameter value, μ_k is the prior mean, and σ_k^2 is its variance. For further technical details, see Appendix A.

5 Results and discussion

The Markov chain Monte Carlo simulations yielded a chain of 500000 samples. From these, 70% from the start of the chain were discarded as warm-up (Fig. 3). A revised posterior distribution obtained by first sampling 10000 entries randomly from the chain, and after that obtaining 1500 entries from those with importance resampling is shown in Fig. 4, and the correlation features are shown in the upper triangle of that figure. For the different processes, Fig. 5 shows an example of the posteriors and the process correlations.

Three different parameter estimates obtained from the posterior distribution were used to look at its features and fluxes: the maximum a posteriori (MAP) estimate, posterior mean estimate, and a "non-hierarchical" posterior mean estimate, where the mean values of the parameters ζ_{exu} (-) and Q_{10} (-) over the different years were used. The "default" parameters in the text and figures refer to values adapted from Raivonen et al. (2017). If not stated otherwise, the maximum a posteriori and posterior mean estimates refer to the values obtained from the importance resampling, not from the MCMC.

5.1 Parameter values

The parameter values used in the analyses are shown in Table 4. The MAP and posterior mean estimates agree on the value of the water-diffusion rate coefficient $f_{D,w}$ (-), and the posteriors shown in Fig. 6 (k) show that the estimates are close to the middle of the marginal distribution, and slightly above the prior value. In tests with a shallower peat column, smaller values of this variable were obtained (not shown).

Contrary to this, the air diffusion rate coefficient $f_{D,a}$ (-) finds its best values lower and the variability of the parameter is larger than for the diffusion rate coefficient in water-filled peat.

The root distribution parameter, λ_{root}, is optimized larger than expected, and again the MAP estimate is close to the posterior mean. This implies that the model optimizes best when the CH_4 produced from the photosynthesis-induced exudate production goes relatively far below the surface: with a value of 0.3, 49% of the roots are deeper than 25cm, 15% of the roots are deeper than 50cm, and just 2.5% are deeper than 75cm, see Fig. 1. In relation to these numbers, the water table depth is most of the time above the depth of -20 cm. Additionally, a larger λ_{root} will facilitate the emission of the CH_4 produced by peat decomposition in the catotelm.

The values of the exudate pool turnover time τ_{exu} are close to the default value of two weeks, with the MAP estimate at a little under 14 days and the posterior mean at two and a half days more. The results from the importance resampling show that the spread is around three days around this posterior mean value. However, the value of $\overline{\zeta_{\mathrm{exu}}}$ controlling amount of exudates produced from photosynthesis, is smaller than the default value at roughly 0.15-0.45 with the MAP and posterior mean estimates at 0.343 and 0.292 respectively. In contrast to this and balancing the effect of a relatively low $\overline{\zeta_{\mathrm{exu}}}$, the parameter $f_{CH_4}^{\mathrm{exu}}$ (-), controlling how much methane is produced from anaerobic decomposition of exudates, has a skewed posterior marginal distribution with most of the mass above the value of 0.7, as can be seen in Fig. 6.

The non-hierarchically optimized parameter V_{O0} (mol m^{-3} s^{-1}) controlling the amount of CH_4 oxidation taking place is close to the minimum allowed value at one fifth of the default value. This is also true for the parameter controlling heterotrophic respiration, V_{R0} (mol m^{-3} s^{-1}), whose all optimized estimates reside close to its minimum value reducing the amount of heterotrophic respiration taking place. The posteriors are very narrow. In contrast to these narrow posteriors, the parameters ΔE_{oxid} (J mol$^-$1) and ΔE_R (J mol^{-1}), which are present in the same equations as the V_{O0} and V_{R0}-parameters, have slightly wider posterior distributions, with the former slightly under and the latter slightly above the default values.

Table 4 shows that the hierarchically optimized parameter Q_{10} (-), controlling the temperature dependence of the CH_4 production from peat decomposition, has slightly different values for the MAP and posterior mean estimates, with the Gibbs-sampled mean value (mean of those values in the case of the posterior mean) at 5.72 and 4.43 respectively.

The parameter τ_{cato} (y), also controlling the peat decomposition rate in the catotelm, compensates for the differences of $\overline{Q_{10}}$ between the MAP and posterior mean estimates by having a faster turnover time for the posterior mean than the MAP estimate. That parameter has a wide posterior, ranging from around 10000 to 30000, which was the value used by Raivonen et al. (2017) and the upper limit of the parameters in our work. Our posterior density goes to zero towards the higher limit, and the posterior mean is found at the value of 22690 years.

The inter-annual variability of Q_{10} (-) is mostly similar for both MAP and posterior mean estimates. For instance the years of the smallest values are 2007 and 2008 in both cases, and the values of the years 2006, 2011, and 2014 are the largest in both cases. For the other hierarchically calibrated parameter, ζ_{exu} (-), these similarities do not exist.

5.2 Costfunction values and model fit

Table 4 lists the costfunction values for the MAP and posterior mean estimates, and the annual errors for the MAP, posterior mean, and non-hierarchical posterior mean estimates and default parameter values are shown for each parameter set in Fig. 7. The costfunction value is unsurprisingly lower for the MAP estimate than for the posterior mean estimate, indicating a better

fit in terms of the error model. In figure Fig. 7 (b) the non-hierarchical posterior estimate shows a large variance of the annual errors, with early years having a positive bias, and later years having a negative bias. Incidentally the average discrepancy from observations over the whole period for the non-hierarchical posterior mean is small for both methane and carbon dioxide, as Fig. 8 indicates. However, the variation for methane is the largest, implying that the annual variation is not reflected well. The model estimates of the annual fluxes are good in that the variance of the errors is small for both MAP and posterior mean experiments, especially, even though the estimates show a negative bias of 25%. Compared to the default parameters, which strongly underestimate methane emissions (and even more overestimate the carbon dioxide emissions), the flux estimates are much improved. This is to be expected as the results shown are not for an independent validation dataset. Rather, the motivation with the MAP and posterior mean estimates is to see how the model fit looks like for optimized parameters and how the features differ from the unoptimized ones. It is, however, worth noting that the target objective function did not aim at minimizing annual discrepancies but daily residuals that were considered correlated.

A cross validation of the regression modeling in terms of the annual errors is shown in Fig. 7 (b) and 8. While the annual estimates are not on average better than the ones from the simulation with the non-hierarchically obtained posterior mean, the spread of the errors are acceptable, particularly if the strong negative bias in 2007, which is mostly due to lack of observations during the season, is disregarded. Additionally the overall biases are surprisingly slightly better than with the optimized parameters, due to effects of the prior, different data resolution in the costfunction, and the non-trivial error model used. The cross validation is described in Sec. 5.6.

The positive bias in the CO_2 may partly be due to the assumption that 70% of the NPP comes from the aerenchymatous plants, and this affected the data that the sqHIMMELI model results were matched with.

All years of hierarchically optimized experiments show at least a small negative annual bias in the methane flux when compared to the available observations. This can be due to the high day to day variability of the summertime fluxes, which dominate year-round total fluxes, and the fact that the model can not, without data about the fine structure and heterogeneity of the wetland, match the high variability fluxes. The proportional model-data residual error component $\alpha\, y_t$ (Appendix A) allows the model to underestimate the high peaks more than the low flux values. The error model favors the baseline of the lower values during periods when observed variance is very high, for instance in the peak emission season of 2010. This is also true for periods of increased ebullition, and such fluxes are very difficult to fit into. These periods contribute to both the costfunction values and the underestimation of the total methane flux. Any temporal shifts of peaks of seasons are penalized heavily, and the optimized parameter values rather produce less peaks than right size peaks at a slightly wrong time.

Another reason is that the carbon dioxide fluxes are overestimated by the model, leading to need to balance between the two, and as methane production in the wetland also produces carbon dioxide, the optimization algorithm will find a middle ground between the conflicting needs of minimizing carbon dioxide and maximizing methane production.

Additionally, the wintertime methane fluxes are underestimated systematically, and the emissions start slightly late in early summer, which produces a negative bias to the total flux even though visually the fit is good, as can be seen in Fig. 9. This figure also reveals that the observations for the vast majority fall within the confidence margins suggested by the ARMA model for

the residual. The variation from the full posterior is higher because the uncertainty shown in Fig. 9 does not take the parameter variations into account.

The carbon dioxide time series against flux observations are shown in Fig. 10. This figure reveals that sqHIMMELI and the error model most of the time are able to explain the carbon dioxide fluxes well, even though some of the largest deviations are not captured. Since in an observational time series outliers can come from an underlying process that is not well explained by these models, having a small number of such deviations is not surprising.

The input data has a role in affecting the model fit to the data, and since NPP is a modeled quantity, there is some additional uncertainty stemming from that modeling involved. For LAI we note that even though in reality it is not identical every year, in the model it follows the same pattern, (see Appendix E). The parameter calibration must then favor parameters producing a good fit in terms of average model performance.

5.3 Parameter values and processes in sqHIMMELI

The sqHIMMELI model produces the CH_4 from anaerobic respiration that originates from peat decay and the decay of root exudates. These production components, along with the different output pathways, CH_4 oxidation and model residuals, are plotted as functions of water table depth in Fig. 11 for the MAP, posterior mean, non-hierarchical posterior mean, and default parameter values. The process correlations and covariances are shown for the year 2012 in Fig. 5.

In the following, *all ebullition* refers to any ebullition in the peat column regardless to whether the bubbles reach the peat column surface. *Ebullition* refers to the part of "all ebullition" which reaches the surface. Most of the time the water table is under the peat surface, and at those times "ebullition" is zero, although "all ebullition" can be substantial. In that case the ebullition flux does not go directly into the atmosphere, but into the first air-filled peat layer above the water table level, and continues from there via other pathways. The reason for this separation comes from implementation details of HIMMELI. In all experiments, ebullition reaching the surface is minor fraction of the total CH_4 emission.

For the posterior mean estimate, the flux components and oxidation are shown as time series in Fig. 12. Optimizing the model leads to increased production of methane from peat decay, as can be seen in Fig. 11 (f). A similar effect is seen also in the plant transport component in Fig. 11 (b).

Comparing results from simulations with optimized parameters to results using the default parameter values (shown in Table 4) shows that the optimization somewhat decreases the role of the plant transport pathway in favor of the diffusion pathway, especially for years 2010, 2011, and 2013. Diffusion and all ebullition fluxes are closely tied to each other, as can be seen in Fig. 7 (a), in that in many years (2007-2008, 2012-2014) their values are close to each other for all estimates. This is also visible in the flux component time series in Fig. 12.

5.3.1 Methane production and oxidation

Figures 13 and 5 show, that there is considerable inter-annual variation in the production of CH_4 from both of the production processes. Year 2007 has a high amount of production from peat decomposition, whereas year 2006 shows a lot less, even though the ζ_{exu}-controlled proportion does not change equally much. Generally, though, in years of high emissions the amount

of CH_4 from both of the production sources is increased. The shape of the NPP input, shown in Fig. 9, does not change remarkably from year to year, but the emissions change considerably, as the model state and input affect the production non-linearly. For example in times of low WTD in the peak emission season, the root exudates do not contribute to CH_4 production as much as during slightly wetter times, as much of the roots are located in the dry part of the peat column and the exudates are deposited there (Fig. 11 (e)). Another explanation for changes in CH_4 production comes through the production-determining parameters, whose variation is in Sec. 5.6 found to be related to the springtime temperature and NPP.

The NPP-based CH_4 production controlled by the parameter ζ_{exu} (-) is not strongly constrained by its hyperprior as can be seen in Fig. 6 (b) and the MAP and posterior mean estimates. The posterior means in table 4 are between 0.182 and 0.323 for the different years. For the MAP values the values are slightly higher, leading to a larger input to the root exudates pool. The effect of ζ_{exu} on the exudate pool sizes can be seen by comparing the posterior mean values to the exudate pool sizes in Fig. 9. The values obtained here are in line of values reported by Walker et al. (2003), who gives a range of roughly 0.15-0.65 in terms of our ζ_{exu}-parameter, when also considering the mean value of the $f_{\mathrm{exu}}^{\mathrm{CH_4}}$. This parameter finds its maximum a posteriori value at 0.729, which is close to the prescribed upper limit of 0.77. The posterior mean is at 0.736. From these results we can conclude that a relatively large portion of the photosynthesized sugar is respired into methane.

The parameter $f_{\mathrm{exu}}^{\mathrm{CH_4}}$ is only affecting the part of the anaerobic respiration generated from root exudates. The two sources of anaerobic respiration (peat decomposition and root exudates) are in sqHIMMELI controlled by two different processes having different sets of parameters. The parameter controlling the peat decomposition, $g_{\mathrm{CH_4}}^{Q_{10}}$, appearing in Eq. 16 and functioning analogously to $f_{\mathrm{exu}}^{\mathrm{CH_4}}$ is set at the value 0.4 based on prior information and this parameter was not part of the calibration. The discrepancy between the $g_{\mathrm{CH_4}}^{Q_{10}}$ and $f_{\mathrm{exu}}^{\mathrm{CH_4}}$ parameters is after the optimization rather large, and therefore in any future calibration of the sqHIMMELI model with flux data from another site or with data from several sites, including this parameter could be also considered. If the value of 0.4 for $g_{\mathrm{CH_4}}^{Q_{10}}$ is an underestimate, the model produces too much carbon dioxide and too little methane from the peat decomposition component. However, since the production processes are correlated in the posterior distribution, as shown in Fig. 5, increasing the value of $g_{\mathrm{CH_4}}^{Q_{10}}$ would also be reflected in decreasing the production of methane from root exudates and increasing the production of carbon dioxide correspondingly. According to Fig. 5, methane oxidation would also be affected by changes to methane production from the root exudate component. Hence excluding the parameter $g_{\mathrm{CH_4}}^{Q_{10}}$ from the optimization does not effect the total CO_2 and CH_4 fluxes in a major way, but the balance of the production processes and methane oxidation can be slightly affected.

The year to year variation of the posterior distributions of the ζ_{exu}-parameter, shown in Fig. 14, is large and this difference has an important role in driving the annual CH_4 production. For especially the years 2007, 2008, 2012 and 2014 the importance resampling has the effect of increasing the value of the parameter, correspondingly increasing the production of methane. This effect is not visible for the other hierarchically modeled production-related parameter, the Q_{10}, whose posterior is not affected by the resampling despite the more permissive prior.

The methane produced by the action of ζ_{exu} is distributed according to the root distribution, whose form is determined by λ_{root} (m). The posterior means reveal, that that the contribution of the prior component of λ_{root} to the costfunction is large. Its values might well be larger with a wider prior and more permissive prior, but in regard to how root distributions are in reality

(Fig. 1), larger values for the parameter would make its interpretation difficult. This parameter affects both how exudates are allocated in the column and how deep the fast plant transportation reaches. Clearly there is a need to reach further down, implying that the model performs more optimally when it transports CH_4 faster to the atmosphere.

The exudate pool size follows the net primary production in Fig. 9 with a delay, as one could expect. According to the modeling, the pool sizes are up to 0.5 moles per square meter, and the exudate pool is depleted from December until the start of the growing season.

The methane production from decomposition of peat in anaerobic conditions is aided by the rather strongly correlated parameters Q_{10} (-) and the catotelm carbon decay half-life τ_{cato} (y) as seen in Fig. 4. The prior means of Q_{10} (-) are mostly inside the 1-σ bounds of the hyperprior, and the temperature dependence of the anaerobic respiration from peat decomposition is close to what was *a priori* expected. The MCMC utilized a rather strict prior, which constrained the parameter exploration somewhat. Despite this, also very low values were proposed.

Methane oxidation is quite steady between the different estimates as can be seen in Fig. 13 - except for the default parameters values, with which the amount of oxidation is several tens of percents more. However, there is considerable inter-annual variability, which seems to be related to the varying production from exudates, as seems to be suggested by Fig. 5, and also by Fig. 13.

The stronger oxidation with the default parameter values can be for it part also linked to the larger V_{O0} (mol m^{-3} s^{-1}) parameter, despite that the other parameter determining oxidation in Eq. 7, ΔE_{oxid}, is slightly lower (50000 vs. 53580 for map and 55750 for posterior mean).

The process correlation figure, Fig. 5 also shows that the exudate and peat decomposition based methane production terms are negatively correlated, and that the exudate based production is roughly 50% stronger than the peat decay source.

The hard prior bounds of V_{O0} (mol m^{-3} s^{-1}) were tight and for example Segers (1998) reports that potential CH_4 oxidation can vary across three orders of magnitude. Hence, also lower proportions of CH_4 oxidation could have been seen with a more permissive prior. This would have then also altered the posteriors of the weakly covarying parameters, most notably λ_{root}.

The parameter V_{R0} (mol m^{-3} s^{-1}) controlling heterotrophic respiration correlates positively with CH_4 production via τ_{exu} (s) (smaller value enhances methane production), but the correlations with $\overline{Q_{10}}$ and τ_{cato} seem to cancel out each other. The correlations of $\overline{\zeta_{\mathrm{exu}}}$ are weak implying that that process is well constrained by the combined CO_2 and CH_4 data. There is also a weak anticorrelation between V_{R0} and ΔE_R, which is to be expected based on Eq. 6.

5.3.2 Plant transport

The amount of plant transport in the calibrated models, shown in Fig. 7 (a), is between 75% and 95% which is just slightly higher than the range of 68-85% reported in Wania et al. (2010) in a study simulating CH_4 emissions for seven boreal peatlands.

The high optimized share of plant transport is mainly due to the high values of the root depth controlling parameter λ_{root} (m) and some of the difference between the MAP and posterior mean estimates in Fig. 7 (a) may be explained by the higher root ending cross section area in the MAP estimate, controlled by parameter ρ (m^2 kg^{-1}). Wania et al. (2010) used the parametrization from Eq. 1 with $\lambda_{\mathrm{root}} = 0.2517$, and the root distribution from the posterior mean estimate is shown alongside

that distribution in Fig. 1. Compared with measurements from Saarinen (1996), the amount of roots at 20-60 cm is exaggerated by all of the optimized parameter values. The model provides a better fit to the data when the root conductance is high. However, the posterior distribution of the root tortuousity parameter in Fig. 6 is almost identical to the prior, so obviously there is no need to maximize plant transport at any cost.

Since the parameters ρ (m^2 kg^{-1}) and τ (m m^{-1}) both affect plant transport and are included in Eq. 8, one could expect them to be tightly coupled. In the posterior, however, they are only slightly correlated, with the correlation coefficient of only 0.12 in Fig. 4. This might be due to ρ having the tendency to be close to its the lower limit. The root-ending area parameter ρ has a notable negative correlation with the air-diffusion coefficient $f_{D,a}$ (-). This follows directly from that increased root ending area increases root conductance, as does faster diffusion through the air-filled aerenchyma cells, via Eq. 8.

5.3.3 Diffusion

The masses of the diffusion coefficient parameters $f_{D,a}$ (-) and $f_{D,w}$ (-) in the posterior distributions (Fig. 6 (j) and (k)) are within the rather permissive priors having the values of 0.8. The parameter $f_{D,w}$ is optimized close to the upper limit of one. Kaiser et al. (2016) note that these parameters are not well known, and use for both of them the value of 0.8. Constraining the model with the CO_2 flux measurements results in the diffusion component not correlating with the amount of methane produced via anaerobic peat decomposition.

5.3.4 Ebullition

Ebullition is very strongly tied to diffusion in the flux estimates with parameters from the posterior, as is shown in Fig. 5. The flux component timeseries in Fig. 12 shows that ebullition to the surface is a small fraction (circa 0-3% with optimized parameters), of the total flux. Similarly, Wania et al. (2010) report almost virtually no ebullition to the surface. This result is highly dependent on the type of the wetland as for instance Kaiser et al. (2016) report high ebullition fluxes for a polygonal tundra in the Siberian permafrost region, where the ice-free soil layer reaches only about 30 cm depth during summer. Variation between different sites is very large and depends on whether the water reaches the surface at times of high CH_4 emission.

Contrasting with this, in the simulations with the non-hierarchically optimized parameters, a major part of the diffusive flux, which comprises around 30% of the total flux for most years, is transported by ebullition (Fig. 8) and diffusion is a major flux component, even though ebullition to the surface accounts for only 5% of the total flux. Since ebullition is a fast timescale process, it was not directly constrained in the optimization with parameters, as preliminary tests revealed that daily data resolution would not be sufficient for this. While finer time resolution data would have been available, using it would not have been feasible as there is not enough knowledge about the fine structure of the wetland and micrometeorological conditions affecting the footprint area of the flux tower. It is reasonable to believe that the deviations from the daily averaged fluxes at a finer time resolution would only look like noise in the residuals not improving our parameter posterior. Despite this, ebullition is controlled indirectly by letting CH_4 production and transport parameters control when the water column has enough CH_4 available for ebullition. This happens when the sum of the partial pressures of dissolved gases is larger than the sum of atmospheric and hydrostatic pressures as shown in Eq. 23. The high ebullition-related proportion of the diffusive flux

strengthens the argument that the likelihood formulation results in model optimizing towards parameter values that support rapid CH_4 transport.

5.4 Parameter and process identifiability

The priors of the hierarchical CH_4 production-related parameters Q_{10} (-) and ζ_{exu} (-) in Fig. 6 (b) and (d) are constrained by the data, as are the hierarchical parameters themselves, shown in Fig. 14. The priors of these distributions are wider than their posteriors, which is also the case for the other production-related parameters τ_{exu} (s) and τ_{cato} (y). Both process descriptions for obtaining the anaerobic respiration are clearly needed for a good model fit, because the parameter posteriors do not have remarkable mass in the regions minimizing either of these processes (hierarchical parameters at the lower bounds or turnover rate parameters τ_{exu} and τ_{cato} at the upper bound). The covariances in Fig. 4 and Fig. 5 show that the two production processes covary slightly, with correlation coefficient -0.32, and hence they are to that extent interchangeable. Reasonable identifiability of the Q_{10}-parameters is not obvious, as for example Müller et al. (2015) optimizing a corresponding parameter end up with the parameter at the lower bound of their prescribed range. However, half of the mass of the production terms in the process correlation plot, Fig. 5, lies within a region that for production from exudates is roughly 10% of the total production and for the production from peat decay of the order of 35%,, and hence the production processes can be said to be well constrained.

The posterior distributions of V_{R0} (mol m^{-3} s^{-1}) show, that sqHIMMELI performs better when the heterotrophic respiration is close to being minimized, which is also aided by a posterior mean value of ΔE_R (J mol^{-1}) that is lower than the prior mean. For the oxidation parameters V_{O0} (mol m^{-3} s^{-1}) and ΔE_{oxid} the situation is different: the former has the tendency of being very small - but the temperature response has the tendency of being stronger with posterior mean and MAP values above the prior mean.

Whereas the fraction of plant transport is stable and high, but still constrained, not all the parameters affecting root conductivity are constrained by the data as the root tortuousity posterior distribution follows very closely the prior form. The root ending cross sectional area, however, is constrained to its lower side despite there being mass also above the prior mean value. For this parameter the importance resampling resulted in a changed posterior in that there is a lot more mass at the higher end of the distribution, as can be seen in Fig. 6 (h). In addition to this difference, the effects of the resampling were mostly minor. Still, the resampling informed that the roots should reside slightly higher in the peat column than suggested by the MCMC, and that the $f_{CH_4}^{\mathrm{exu}}$ is constrained to a higher value by the data than suggested by the initial MCMC run.

The transport pathways are well identified as can be seen in the ranges of variation in the transport characteristics in Fig. 5. Notably the transport processes do not strongly anticorrelate implying that they are not obviously interchangeable with each other. The correlation between oxidation and plant transport suggest that uncertainty in oxidation is a major part of the uncertainty in the plant transport portion. On the other hand, there is uncertainty in the absolute magnitude of the total flux (in terms of the posterior uncertainty) and this is reflected in the strong positive correlation between plant transport and the total flux. Similar but weaker positive correlations exist between the total flux and diffusion and ebullition, which is to be expected. The variation of oxidation is around ten percent of the total flux.

5.5 Low WTD in 2006, 2010, and 2011

The calibrated sqHIMMELI model is able to describe the CH_4 flux correctly in times of low water table, which is not obvious as other studies have indicated the challenges in parametrizations of emission models with respect to the water table depth (e.g. Zhu et al. (2014)). Figure 11 shows how the model processes are described under water stress. In times of a very low water table, the plant transport component and methane production from root exudates are decreased somewhat, as is methane oxidation. This results directly from how the model is constructed as exudate deposition to the peat column is allocated depth-wise according to the root density profile. That the model continues to perform well during these years, implies that this method of regulating methane emissions during dry seasons is realistic. The residuals in Fig. 11 (h) further show that there is a only a slight positive emission bias at the times of the very lowest water table levels.

5.6 Predicting emissions with sqHIMMELI

Modeled CH_4 flux estimates may have large errors as was shown in Fig. 8 with the default parameter set. The negative biases in the calibration phase that were found with the maximum a posteriori and posterior mean estimates are reasonable since the quality of the modeled input data from e.g. a land surface scheme will also contribute to the uncertainty in the model predictions. Additionally, a known constant bias can be relatively easily accounted for if the inter-annual variability is correctly modeled.

Compared to the estimate with the optimized annual variations of the methane production related parameters, the non-hierarchical posterior mean estimate produces reasonable flux estimates over the assessment period, with twice the variability in fluxes compared to the posterior mean estimate, even though the average of the errors is closer to zero. The variability is seen in Fig. 7. The hierarchical posterior mean on the other hand does produce very steady estimates of the CH_4 flux compared with observations even though there is a downward bias of 23%, and the smaller inter-annual variance implies better predictive skill. The same is true to a lesser extent also for the maximum a posteriori estimate.

In order to be able to utilize the information regarding the annual variability in the posterior mean estimate for the future prediction of CH_4 emissions, the values of the hierarchical parameters need to be estimated for the simulation years. A simple regression analysis of the hierarchical variables with respect to relevant input data was performed in order to find out if such estimation is possible. As the explaining variables, means, minimums, and maximums of NPP, water table depth, and soil temperature at different depths and over different periods of time were looked at. These time periods were June, July, August, and various different amounts of days from the start of the year.

The analysis revealed that the mean soil temperature of the first 10 weeks (70 days) of the year at the depth of 30-40 cm, denoted here by $\overline{T^{70}_{30-40}}$, is the best single-variable predictor of the Q_{10}-value for that year, and for ζ_{exu}, it is the sum of NPP from the first 130 days of the year, denoted by NPP^{130}. This is hardly surprising, since the peat decomposition process regulated by the parameter Q_{10} is driven by soil temperature, and the anaerobic respiration from exudates controlled by the parameter ζ_{exu} is driven by the NPP input. These variables also indicate that the timing of the start of the growing season might

play a role in determining the parameters. Possible mechanisms could include e.g. effects of the start of growing season on development of the microbe populations in the spring. However, further analysis would be needed to confirm this..

The p values summarizing the reliabilities of the regressions and the r^2 values, which are the coefficients of determination of the fit, are presented in table 5. The r^2 values explain what fraction of the variance of the dependent (predicted) variable is explained by the independent (explaining) variables. The p- and r^2-values uncover that the hierarchical modeling reveals a clear-cut reliable relationship between the early NPP and the optimal ζ_{exu}-parameter ($p = 5 \times 10^{-6}$, $r^2 = 0.957$). This provides new insight into future model development and exemplifies why such a hierarchical description of variables is valuable in Bayesian optimization in a geophysical model context.

For the other inter-annually changing parameter, Q_{10}, the soil temperatures explain only slightly over half of the variation ($p = 0.0185$, $r^2 = 0.571$). Since the effect of this parameter is very important for the total methane flux, this results leaves lots of room for further analysis.The hierarchical parameters Q_{10} and ζ_{exu} for each year can be estimated with

$$Q_{10} = 3.86\,\overline{T^{70}_{30-40}} + 1.76 \tag{25}$$

$$\zeta_{\mathrm{exu}} = -46500 NPP^{130} + 0.431 \tag{26}$$

where the temperatures are in °C, and the units of NPP are mol m^{-2} s^{-1}.

A leave one out-cross validation (LOO-CV, see e.g. Gelman et al. (2013)) of the regression modeling was performed by optimizing the hierarchical parameters with respect to the costfunction in Eq. 24 leaving one year at a time out, calculating the estimates for the hierarchical parameters based on the results obtained for other years, and predicting the CH_4 emissions for the year that was left out. The results of the cross validation are shown in Fig. 7 (b) and 8. The cross-validated results are comparable in terms of annual performance to the non-hierarchical posterior mean. Despite the relatively good performance of the non-hierarchical posterior mean simulation, we note that the cross-validated result should be more relied on for prediction, since the well-predictable ζ_{exu}-parameters contain useful information that is not available in the non-hierarchical posterior mean estimate. A hybrid between these approaches could be also used, using the regression modeled values for the ζ_{exu}-parameters and the mean for the Q_{10}, to minimize the risk of major annual biases due to unsuccessful prediction of the Q_{10}-parameters.

As Fig. 7 (b) shows, much of the error in the cross validation actually comes from challenges estimating year 2007, which is missing the peak season observations, and therefore the error percentage (in terms of the annual observed flux) is easily high, especially as the start of season is modeled with a delay, which is readily apparent in Fig. 9, and in this sense the negative bias in Fig. 7 gives an unnecessarily pessimistic view of the model performance. For the CO_2 fluxes, it can be noted that there is a persistent positive bias of some tens of percents, but the observations are very noisy and due to the processing for the use in the costfunction, they might have biases. The effect of a small bias on the parameter posterior distribution is, however, minor, since the carbon dioxide observations were given less weight in the costfunction than the methane observations. Hence, given their uncertainty the optimized fit to the measurement data can, also in the cross-validation as in the other experiments, be seen as acceptable.

6 Conclusions

In this study, Bayesian calibration of a new process-based wetland CH_4 emission model, sqHIMMELI, was performed using Markov chain Monte Carlo methods, hierarchical statistical modeling of methane production related parameters, Box-Jenkins-type timeseries modeling, and importance resampling, against daily methane and carbon dioxide flux data from the Siikaneva flux measurement site in Finland. The results show that the modeled processes and the estimated parameters are identifiable with the flux data. The parameter correlations and process correlations from random sampling the posterior reveal that there are no redundant processes in the model description. However, a few strong correlations between parameters exist reminding of the difficulty of strictly interpreting parameter values to be connected to isolated physical processes. The optimized model fits well to the data in that the modeled fluxes fit within a range from the data that is expected based on the error modeling.

Preliminary results obtained also suggest that estimation of the annual variation of the parameters controlling methane production from anaerobic respiration of root exudates is feasible and may help to improve the future estimates of the boreal wetland CH_4 emissions.

For future studies, combining observations from several sites and optimizing them together with the methods presented here in conjunction with independent validation can provide valuable information about the uncertainties related to wetland emission modeling and about how to best improve the quality of predicting wetland methane emissions in land surface schemes of climate models.

7 Code availability

The HIMMELI source code is available as a supplement to the publication Raivonen et al. (2017).

8 Data availability

The model input data and the flux measurement data are available upon a reasonable request from the lead author.

Appendix A: Error model for residuals

In section 4.2.1 we described the error models as AR(1) / ARMA(2,1) models where the residuals are Laplace-distributed. Intuitively these models can be thought of as characterizing the "inertia" or "memory" in the model-observation discrepancy. Formally the observation equation for our statistical inference problem can be written as

$$\boldsymbol{y}_t = \boldsymbol{x}_t + \boldsymbol{r}_t^* \tag{A1}$$

$$\boldsymbol{x}_t = M(\boldsymbol{x}_{t-1}, \boldsymbol{z}_{t-1}, \boldsymbol{\theta}) \tag{A2}$$

The vector notation for $\boldsymbol{y}$ and $\boldsymbol{r}^*$ in Eq. A1 refers to that at each time t there can be observations of both methane and carbon dioxide, and M in Eq. A2 denotes the model (sqHIMMELI) advancing the model state $\boldsymbol{x}_{t-1}$ forward in time. The term $\boldsymbol{z}_{t-1}$

is the external model forcing data. In this context, the *error model* that is referred to in text refers to how the $\boldsymbol{r}_t^*$-terms are modeled. The modeling is different for the MCMC and importance resampling steps.

Residuals terms for MCMC

For both CO_2 and CH_4, let $y'_t = \max(c_t, y_t)$, where c_t is the 14-day running mean of the gap-filled flux observations y_t. Due to the heteroscedasticity of the model error, we scale the residuals for error modeling by dividing each model prediction and observation with $\alpha|y'_t| + \gamma$, where α and γ are pre-determined constants. The error-scaled residual at time t is then

$$r_t = \frac{r_t^*}{\alpha|y'_t| + \gamma}. \tag{A3}$$

Let ϕ denote the lag-1 autocorrelation coefficient, meaning the correlation of the residual timeseries with the same residual timeseries one day later. The AR(1)-corrected residual for time t then becomes

$$r_t = \phi\, r_{t-1} + \epsilon_t. \tag{A4}$$

The reason for the way of constructing $\boldsymbol{y}'$ above was to allow for a reasonable amount of error both in the case when there is an emission spike upwards and when the same happens downwards, avoiding the problems when if in the summer there is suddenly a day with zero CH_4 emissions, the observation would be taken to be extremely precise (as $\alpha\, y_t$ would be small) even though the low value is rather due to noise.

The MCMC experiment was performed with a costfunction that permissively allowed for exploration of the parameter space. The α and γ were 0.4 and 0.00075 for CH_4 and 1.0 and 0.029 for CO_2, respectively, and the lag-1 autocorrelation coefficient used was 0.6. Uncertainties motivating such a permissive error description include uncertainties in the NPP model, inadequacies in the model description of the peat column and lack of spatial heterogeneity in the model description, filled gaps in the water table depth data, errors from interpolation of the soil temperature data and heat transfer, and other unknown error sources. The same model error description was used for all MCMC model simulations.

Residuals for importance resampling

The sum of the absolute values of the ϵ_t-terms appears in the objective function, Eq. 24, but the AR(1)-modeled values are in the end not independent and do not accurately follow the Laplace distribution, in part because generous values were chosen for α and γ that allowed for easier exploration of the parameter space. The objective function used for importance resampling fixes these problems.

For choosing the order of autoregressive moving average model (the ARMA(p, q) model), the different models up to order $p = q = 4$ were fitted, and the one whose fitting yielded the lowest Bayesian Information Criterion was picked. After making sure that the fitted residuals are independent by calculating the Durbin-Watson statistic, the order of $(p, q) = (2, 1)$ was chosen. In place of Eq. A4, the error model for the residuals is then written as

$$r_t = \phi_1\, r_{t-1} + \phi_2\, r_{t-2} + \theta\epsilon_{t-1} + \epsilon_t, \tag{A5}$$

where the ϕ-parameters are the AR model parameters and the θ is the MA-part.

The scaling of the model residuals for choosing the ARMA parameters and the values for α and γ above (separately for the CH_4 and CO_2 timeseries) was done by effectively calculating the 2-week running mean of the variances of the flux from observations for each day of year. More explicitly, let

$$\hat{y}_t = \sqrt{(\mathbb{V}_{\mathrm{doi}=t}[y_t])} \tag{A6}$$

denote the standard deviation of the observed fluxes for a given day of year over the whole observation dataset. Then the residuals are scaled as before by

$$r_t = \frac{r_t^*}{\alpha \boldsymbol{h}^T \hat{\boldsymbol{y}}_t + \gamma} \tag{A7}$$

where $\boldsymbol{h}^T$ is a vector of length 14 with each element having value $\frac{1}{14}$ and $\hat{\boldsymbol{y}}_t$ is the vector with elements $\hat{y}_{t-7}, \ldots, \hat{y}_{t+6}$. Let $\Psi(b_i)$ denote the value of a discretization of the standard Laplace distribution at point $b_i \in \{b_1, \ldots, b_{N_b}\}$, and let $S_{\alpha,\beta}^{\tilde{\phi}_1,\tilde{\phi}_2,\tilde{\theta}}(b_i)$ denote the empirical probability density function of the set of the transformed residual terms, the ϵ_t-terms in Eq. A5, again at point b_i. The parameters $\tilde{\phi}_1, \tilde{\phi}_2$, and $\tilde{\theta}$ are the optimized ARMA model parameters from fitting the model.

The ARMA(2,1) model parameters and the parameters α and γ are determined for the importance resampling by minimizing the *Kullback-Leibler divergence*,

$$D_{KL}(\Psi \| S_{\alpha,\gamma}^{\tilde{\phi}_1,\tilde{\phi}_2,\tilde{\theta}}) = -\sum_{i=1}^{i=N_b} \log \Psi(b_i) \frac{S_{\alpha,\gamma}^{\tilde{\phi}_1,\tilde{\phi}_2,\tilde{\theta}}(b_i)}{\Psi(b_i)}, \tag{A8}$$

which is a measure of similarity between distributions. Effectively we fit the error model parameters to make sure that the modeled residuals really are Laplace-distributed and independent. The parameters α and γ are then chosen to be

$$\alpha, \gamma = \underset{\alpha,\gamma}{\operatorname{argmin}} D_{KL}(\Psi \| S_{\alpha,\gamma}^{\tilde{\phi}_1,\tilde{\phi}_2,\tilde{\theta}}), \tag{A9}$$

and the ARMA-parameters are chosen to be the ones from the model fit with those parameters α and γ minimizing the KL-divergence. The BOBYQA optimization algorithm (Powell, 2009) was used to carry out the minimization. The procedure was performed for 50 parameters vectors randomly sampled from the posterior of the MCMC run and the medians of these values, which were for all parameters narrowly distributed, were the final ones picked for the likelihood used in importance resampling. The actual values of these parameters for methane were: $\alpha^{\mathrm{CH_4}} = 0.594$, $\gamma^{\mathrm{CH_4}} = 1.38 \times 10^{-6}$, $\phi_1^{\mathrm{CH_4}} = 1.30$, $\phi_2^{\mathrm{CH_4}} = -0.325$, and $\theta^{\mathrm{CH_4}} = -0.770$; correspondingly for carbon dioxide $\alpha^{\mathrm{CO_2}} = 0.443$, $\gamma^{\mathrm{CO_2}} = 3.96 \times 10^{-3}$, $\phi_1^{\mathrm{CO_2}} = 1.21$, $\phi_2^{\mathrm{CO_2}} = -0.242$, and $\theta^{\mathrm{CO_2}} = -0.738$. The histograms of the ϵ_t-values and the autocorrelation functions are shown in Fig. 2.

Appendix B: A basic outline of MCMC

Markov chain Monte Carlo (MCMC) methods are a class of Bayesian methods that can be used for obtaining the probability distribution $p(\boldsymbol{\theta}|\boldsymbol{y})$ for a parameter vector $\boldsymbol{\theta} \in \boldsymbol{R}^n$ given data $\boldsymbol{y} \in \boldsymbol{R}^k$. According to Bayes' theorem, this can be written as

$$p(\boldsymbol{\theta}|\boldsymbol{y}) = \frac{p(\boldsymbol{y}|\boldsymbol{\theta})p(\boldsymbol{\theta})}{p(\boldsymbol{y})}, \tag{B1}$$

where $p(\boldsymbol{y}|\boldsymbol{\theta})$ is the *likelihood* (in this work the first two terms on the right hand side of Eq. 24), and $p(\boldsymbol{\theta})$ is the *prior* (the last term). The *evidence*, $p(\boldsymbol{y})$ is often very difficult to evaluate, but in MCMC this is not needed, because MCMC algorithms evaluate ratios of successive evaluations of $p(\boldsymbol{\theta}|\boldsymbol{y})$, making the denominators to cancel out and hence the evidence term can be dropped.

MCMC sampling starts by taking some starting value $\boldsymbol{\theta}$ and calculating the objective function (also known as *costfunction*) value $J(\boldsymbol{\theta}) \in \mathbb{R}$ - the notation here is the same as in Eq. 24. The algorithm then draws a new sample of the parameter vector, $\boldsymbol{\theta'}$ from a prescribed *proposal distribution* $q(\boldsymbol{\theta})$, and evaluates $J(\boldsymbol{\theta'})$. It accepts the new parameter vector with a probability that depends on the value of $J(\boldsymbol{\theta'})$ and the objective function value of the previous accepted parameter, $J(\boldsymbol{\theta})$. If the value is accepted, the chain will move to position $\boldsymbol{\theta'}$ (setting $\boldsymbol{\theta} \leftarrow \boldsymbol{\theta'}$), and if $\boldsymbol{\theta'}$ is rejected, the value $\boldsymbol{\theta}$ will be repeated in the chain. After this a new value, sampled from $q(\boldsymbol{\theta})$ (which is possibly a different distribution from the one used at the previous iteration as $\boldsymbol{\theta}$ may have changed) will be proposed and the whole process is repeated. In the end the procedure will produce a chain of parameter values.

According to Markov chain theory, the sampled parameter values will eventually follow the *target distribution* $p(\boldsymbol{\theta}|\boldsymbol{y})$ meaning, that in such a case picking a random element from the chain amounts to drawing a sample directly from the target distribution. As real-life Markov chains are of finite length, the *posterior distribution* obtained from the chain is an approximation of the underlying target distribution.

In practice this means, that with MCMC it is possible to find a good approximation of the probability density function of the parameter vector $\boldsymbol{\theta}$ in cases, where the model is not suitable for analytical treatment. From this probability density function, valuable information such as modes, variances, and correlations of the parameters can be analyzed. The posterior also reveals, what parameters are constrained by the data, and what are not.

For efficient convergence of the chain to the posterior distribution a good estimate of $q(\boldsymbol{\theta})$ is needed. The Adaptive Metropolis algorithm automatically calibrates the proposal during the MCMC.

Appendix C: Metropolis within Gibbs sampling of the parameters

The hierarchical parameters Q_{10}^{year} and $\zeta_{\mathrm{exu}}^{\mathrm{year}}$ are denoted here generically by θ^i, where i refers to the different years. The priors of these parameters are defined by the *hyperparameters* μ_i and σ_i that determine the prior of θ^i by

$$\theta^i \sim N(\mu_i, \sigma_i^2). \tag{C1}$$

The unknown hyperparameters μ_i and σ_i^2 have probabilistic models

$$\mu_i \sim N(\mu_0, \tau_0^2) \tag{C2}$$

$$\sigma_i^2 \sim \text{Inv-}\chi^2(n_0, \sigma_0^2), \tag{C3}$$

where μ_0 and τ_0^2 define the mean and variance of the hyperprior of μ_i, $n_0 \in \mathbb{N}$ defines the number of degrees of freedom of the Inv-χ^2 distribution, and σ_0^2 is the expected value of the scaled Inv-χ^2 distribution.

In Gibbs sampling the full conditional posterior distributions of the hyperparameters and the parameters θ_i are sampled in turns. Due to the conjugacy of the normal distribution and the scaled Inv-χ^2 distribution, closed form expressions exists for sampling from $p(\mu_i|\sigma^2,\mu_0,\sigma_0^2,\theta^i)$ and $p(\sigma_i^2|\sigma_0^2,n_0,\theta^i)$, where μ is the current mean of the parameters θ_i and σ^2 is their variance. The Gibbs sampling therefore consists of three steps:

1. Draw μ_i from

$$\mu_i|\mu,\sigma^2 \sim N\left(\frac{\frac{n_i\overline{\theta^i}}{\sigma^2}+\frac{\mu_0}{\tau_0^2}}{\frac{n_i}{\sigma^2}+\frac{1}{\tau_0^2}}, \frac{1}{\frac{n_i}{\sigma^2}+\frac{1}{\tau_0^2}}\right), \tag{C4}$$

2. draw σ_i^2 from

$$\sigma_i^2|\boldsymbol{\theta},\boldsymbol{\mu} \sim \text{Inv}-\chi^2\left(n_0+n_i, \frac{\sigma_0^2 n_0+\sum_{j=1}^{n_i}(\theta_j^i-\mu_j)^2}{n_0+n_i}\right), \text{ and} \tag{C5}$$

3. draw the parameters θ_i (and the non-hierarchical parameters) with MCMC, since closed-form expression for $p(\boldsymbol{\theta}|\phi,\boldsymbol{y})$, where ϕ denotes all the different hyperparameters, is not available.

In this work, the value of the parameter τ_0^2 was set to the value of σ_0^2, n_i is the number of years, and the value of n_0 was set to 9. The means and variances obtained this way describe the interannual variability of the parameters, and not including them as parameters in the MCMC sampling reduces the dimension of space that the MCMC sampler needs to explore, speeding up convergence of the posterior distribution.

Appendix D: Importance resampling

Importance resampling is a method for obtaining samples from a desired (unnormalized) distribution $q(\boldsymbol{\theta})$ by re-evaluating samples from a similar distribution from which it is know how samples are generated, $p(\boldsymbol{\theta})$. It is usually remarkably faster than for instance re-performing an MCMC experiment.

The samples $\boldsymbol{\theta}_1 \ldots \boldsymbol{\theta}_N$ are first drawn from $p(\boldsymbol{\theta})$ (in our case randomly picked from the MCMC chain), and at these points the new posterior density $q(\boldsymbol{\theta})$ is evaluated. For each of these, the *weights* are defined by $w(\boldsymbol{\theta}_i)=\frac{q(\boldsymbol{\theta}_i)}{p(\boldsymbol{\theta}_i)}$. The samples from the distribution $q(\boldsymbol{\theta})$ are then generated by sampling according to the set of normalized weights, $\tilde{w}(\boldsymbol{\theta}_i)=\frac{w(\boldsymbol{\theta}_i)}{\sum_{j=1}^{N} w(\boldsymbol{\theta}_j)}$. The sampling is performed without replacement. For further details, see e.g. Gelman et al. (2013).

Appendix E: NPP and LAI

We estimated the net photosynthesis rate, P_n, of vascular plants of Siikaneva for years 2005-2014 by utilizing regression models of gross photosynthesis, P_g, and autotrophic respiration R_a formulated for peatland vegetation (Riutta et al., 2007a, b; Raivonen et al., 2015). The model of the P_g of sedge and dwarf shrub canopy (Riutta et al., 2007a) simulates the carbon

uptake driven by photosynthetically active radiation (PAR), WTD and air temperature. The model of R_a (Raivonen et al., 2015) simulates the respiration rate driven by air temperature and WTD and was parameterized for sedges only.

Both P_g and R_a models simulate the carbon fluxes per soil surface area and the rate depends on the LAI. We simulated the LAI using a lognormal function presented by (Wilson et al., 2007). Parameter values of the LAI model were obtained by averaging the values reported by (Wilson et al., 2007) for the vascular species abundant at Siikaneva. For the growing season peak LAI we used the maximum LAI observed at the eddy covariance footprint area, viz. approximately 0.4 m^2 m^{-2} (Riutta et al., 2007b). We also included a constant wintertime LAI since a significant green sedge biomass may overwinter, approximately 15% of the maximum (Saarinen, 1998; Bernard and Hankinson, 1979). The overwintering LAI at Siikaneva would thus be 0.05 m^2 m^-2 . The same LAI was used for all the years and this LAI also was given as the input for the CH_4 transport model.

The daily averages of P_n were calculated by subtracting R_a from P_g. The models were run with measured meteorological data. We determined the photosynthetically active seasons based on snowmelt dates in spring or arrival of snowcover in autumn from the reflected PAR data, or based on air temperature (permanently greater than 5 °C assumed to be the growing season). After the calculation, we compared the resulting P_n of vascular vegetation of year 2005 to eddy covariance CO_2 fluxes from Siikaneva. We used the GPP derived from the measured NEE by (Aurela et al., 2007). The GPP was on average 4.5-fold compared with our P_n , with a R^2 of 0.9. GPP also includes the photosynthesis of *Sphagnum* mosses as well as CO_2 released in autotrophic respiration. *Sphagnum* accounted for 20-40% of the GPP in the study by (Riutta et al., 2007a) and autotrophic respiration has been observed to be roughly 50% of GPP (Gifford, 1994). Consequently, the NPP of vascular vegetation can be estimated by multiplying the GPP with 0.7×0.5. This estimate was still 1.56-fold compared with the P_n for the year 2005. Since the P_n also was lower than generally reported for peatlands, we chose to trust the eddy covariance measurement and scaled the P_n of all the years upwards by multiplying with 1.56. For further details, please consult Raivonen et al. (2017).

Author contributions. JS designed the study with help from the co-authors, programmed the algorithms, performed the model simulations, analyzed the results, and prepared the manuscript and the figures. MR provided and validated the input data and helped with the interpretation of the results. LB contributed several model subroutines and helped to interpret the results. ML provided assistance with getting the technical aspects of the Bayesian analysis right. OP provided insight into the data used. JM, TV, and TA provided helpful critical comments and suggestions that helped to improve the manuscript substantially.

Competing interests. The authors state that they are free from any conflicting interests.

Acknowledgements. We would like to thank the University of Helsinki researchers M.Sc. Pavel Alekseychik, and Dr. Ivan Mammarella, and Prof. Janne Rinne from Lund University for valuable comments and input regarding the Siikaneva measurement site data. We would also like to thank Prof. Heikki Haario from Lappeenranta University of Technology, Dr. Janne Hakkarainen from Finnish Meteorological Institute, and Prof. Samuli Siltanen from University of Helsinki for comments regarding the mathematical aspects of the study.

This work has been supported by the EU LIFE+ project MONIMET LIFE12 ENV/FI/000409, and the EU FP7 project EMBRACE. We additionally acknowledge funding from the RED platform of the Lappeenranta University of Technology, and thank the Academy of Finland Center of Excellence (272041), CARB-ARC (285630), ICOS Finland (281255) ICOS-ERIC (281250), NCoE eSTICC (57001), EU-H2020 CRESCENDO (641816) and Academy Professor projects (284701) and (282842).

References

Arah, J. R. M. and Stephen, K. D.: A Model of the Processes Leading to Methane Emission from Peatland, Atmospheric Environment, 32, 1998.

Aurela, M., Tuovinen, J.-P., and Laurila, T.: Net CO2 exchange of a subarctic mountain birch ecosystem, Theoretical and Applied Climatology, 70, 135–148, doi:10.1007/s007040170011, https://doi.org/10.1007/s007040170011, 2001.

Aurela, M., Riutta, T., Laurila, T., Tuovinen, J.-V., Vesala, T., Tuittila, E.-S., Jinne, J., Haapanala, S., and Laine, J.: CO2 exchange of a sedge fen in southern Finland—the impact of a drought period, Tellus B, 59, 826–837, doi:10.1111/j.1600-0889.2007.00309.x, http://dx.doi.org/10.1111/j.1600-0889.2007.00309.x, 2007.

Bellisario, L. M., Bubier, J. L., Moore, T. R., and Chanton, J. P.: Controls on CH4 emissions from a northern peatland, Global Biogeochemical Cycles, 13, 81–91, doi:10.1029/1998GB900021, http://dx.doi.org/10.1029/1998GB900021, 1999.

Bergman, I., Klarqvist, M., and Nilsson, M.: Seasonal variation in rates of methane production from peat of various botanical origins: effects of temperature and substrate quality, FEMS Microbiology Ecology, 33, 181–189, doi:10.1111/j.1574-6941.2000.tb00740.x, http://dx.doi.org/10.1111/j.1574-6941.2000.tb00740.x, 2000.

Bernard, J. M. and Hankinson, G.: Seasonal Changes in Standing Crop, Primary Production, and Nutrient Levels in a Carex rostrata Wetland, Oikos, 32, 328–336, http://www.jstor.org/stable/3544743, 1979.

Bohn, T. J., Melton, J. R., Ito, A., Kleinen, T., Spahni, R., Stocker, B. D., Zhang, B., Zhu, X., Schroeder, R., Glagolev, M. V., Maksyutov, S., Brovkin, V., Chen, G., Denisov, S. N., Eliseev, A. V., Gallego-Sala, A., McDonald, K. C., Rawlins, M. A., Riley, W. J., Subin, Z. M., Tian, H., Zhuang, Q., and Kaplan, J. O.: WETCHIMP-WSL: intercomparison of wetland methane emissions models over West Siberia, Biogeosciences, 12, 3321–3349, doi:10.5194/bg-12-3321-2015, https://www.biogeosciences.net/12/3321/2015/, 2015.

Chatfield, C.: The analysis of time series: an introduction, Chapman and Hall, 4th edn., 1989.

Ciais, P., Sabine, C., Bala, G., Bopp, L., Brovkin, V., Canadell, J., Chhabra, A., DeFries, R., Galloway, J., Heimann, M., Jones, C., LeQuere, C., Myneni, R., Piao, S., and Thornton, P.: Carbon and Other Biogeochemical Cycles, book section 6, p. 465–570, Cambridge University Press, Cambridge, United Kingdom and New York, NY, USA, doi:10.1017/CBO9781107415324.015, www.climatechange2013.org, 2013.

Cresto Aleina, F., Runkle, B. R. K., Brücher, T., Kleinen, T., and Brovkin, V.: Upscaling methane emission hotspots in boreal peatlands, Geoscientific Model Development, 9, 915–926, doi:10.5194/gmd-9-915-2016, http://www.geosci-model-dev.net/9/915/2016/, 2016.

Davidson, E. A., Janssens, I. A., and Luo, Y.: On the variability of respiration in terrestrial ecosystems: moving beyond Q10, Global Change Biology, 12, 154–164, doi:10.1111/j.1365-2486.2005.01065.x, http://dx.doi.org/10.1111/j.1365-2486.2005.01065.x, 2006.

Frolking, S., Talbot, J., Jones, M. C., Treat, C. C., Kauffman, J. B., Tuittila, E.-S., and Roulet, N.: Peatlands in the Earth's 21st century climate system, Environmental Reviews, 19, 371–396, doi:10.1139/a11-014, http://dx.doi.org/10.1139/a11-014, 2011.

Gedney, N., Cox, P. M., and Huntingford, C.: Climate feedback from wetland methane emissions, Geophysical Research Letters, 31, n/a–n/a, doi:10.1029/2004GL020919, http://dx.doi.org/10.1029/2004GL020919, l20503, 2004.

Gelman, A., Carlin, J., Stern, H., Dunson, D., Vehtari, A., and Rubin, D.: Bayesian Data Analysis, Chapman and Hall/CRC, 3rd edn., 2013.

Gifford, R. M.: The Global Carbon Cycle: a Viewpoint on the Missing Sink, Functional Plant Biology, 21, 1–15, http://dx.doi.org/10.1071/PP9940001, 1994.

Grant, R. F. and Roulet, N. T.: Methane efflux from boreal wetlands: Theory and testing of the ecosystem model Ecosys with chamber and tower flux measurements, Global Biogeochemical Cycles, 16, 2–1–2–16, doi:10.1029/2001GB001702, http://dx.doi.org/10.1029/2001GB001702, 1054, 2002.

Haario, H., Saksman, E., and Tamminen, J.: An Adaptive Metropolis Algorithm, Bernoulli, 7, 223–242, 2001.

Hararuk, O., Xia, J., and Luo, Y.: Evaluation and improvement of a global land model against soil carbon data using a Bayesian Markov chain Monte Carlo method, Journal of Geophysical Research: Biogeosciences, 119, 403–417, doi:10.1002/2013JG002535, http://dx.doi.org/10.1002/2013JG002535, 2013JG002535, 2014.

Hornibrook, E. R., Longstaffe, F. J., and Fyfe, W. S.: Spatial distribution of microbial methane production pathways in temperate zone wetland soils: Stable carbon and hydrogen isotope evidence, Geochimica et Cosmochimica Acta, 61, 745 – 753, doi:http://dx.doi.org/10.1016/S0016-7037(96)00368-7, http://www.sciencedirect.com/science/article/pii/S0016703796003687, 1997.

IPCC: Summary for Policymakers, book section SPM, p. 1–30, Cambridge University Press, Cambridge, United Kingdom and New York, NY, USA, doi:10.1017/CBO9781107415324.004, www.climatechange2013.org, 2013.

Joabsson, A. and Christensen, T. R.: Methane emissions from wetlands and their relationship with vascular plants: an Arctic example, Global Change Biology, 7, 919–932, doi:10.1046/j.1354-1013.2001.00044.x, http://dx.doi.org/10.1046/j.1354-1013.2001.00044.x, 2001.

Juottonen, H.: Archaea, Bacteria, and methane production along environmental gradients in fens and bogs, Ph.D. thesis, University of Helsinki, 2008.

Kaiser, S., Beer, C., Göckede, M., Castro-Morales, K., Knoblauch, C., Ekici, A., Kleinen, T., Zubrzycki, S., Sachs, T., and Wille, C.: Process-based modelling of the methane balance in periglacial landscapes with JSBACH, Geoscientific Model Development Discussions, 2016, 1–47, doi:10.5194/gmd-2016-103, http://www.geosci-model-dev-discuss.net/gmd-2016-103/, 2016.

Kirschke, S., Bousquet, P., Ciais, P., Saunois, M., Canadell, J. G., Dlugokencky, E. J., Bergamaschi, P., Bergmann, D., Blake, D. R., Bruhwiler, L., Cameron-Smith, P., Castaldi, S., Chevallier, F., Feng, L., Fraser, A., Heimann, M., Hodson, E. L., Houweling, S., Josse, B., Fraser, P. J., Krummel, P. B., Lamarque, J. F., Langenfelds, R. L., Le Quere, C., Naik, V., O'Doherty, S., Palmer, P. I., Pison, I., Plummer, D., Poulter, B., Prinn, R. G., Rigby, M., Ringeval, B., Santini, M., Schmidt, M., Shindell, D. T., Simpson, I., Spahni, R., Steele, L. P., Strode, S. A., Sudo, K., Szopa, S., van der Werf, G. R., Voulgarakis, A., van Weele, M., Weiss, R. F., Williams, J. E., and Zeng, G.: Three decades of global methane sources and sinks, Nature Geoscience, 6, 813–823, doi:10.1038/ngeo1955, <GotoISI>://WOS:000325003700010, n/a, 2013.

Kullback, S. and Leibler, R. A.: On Information and Sufficiency, Ann. Math. Statist., 22, 79–86, doi:10.1214/aoms/1177729694, https://doi.org/10.1214/aoms/1177729694, 1951.

Lai, D.: Methane Dynamics in Northern Peatlands: A Review, Pedosphere, 19, 409 – 421, doi:http://dx.doi.org/10.1016/S1002-0160(09)00003-4, http://www.sciencedirect.com/science/article/pii/S1002016009000034, 2009a.

Lai, D. Y. F.: Modelling the effects of climate change on methane emission from a northern ombrotrophic bog in Canada, Environmental Geology, 58, 1197–1206, doi:10.1007/s00254-008-1613-5, http://dx.doi.org/10.1007/s00254-008-1613-5, 2009b.

Laine, M.: Adaptive MCMC methods with applications in environmental and geophysical models, Ph.D. thesis, Lappeenranta University of Technology, 2008.

Lehtonen, I., Ruosteenoja, K., and Jylhä, K.: Projected changes in European extreme precipitation indices on the basis of global and regional climate model ensembles, International Journal of Climatology, 34, 1208–1222, doi:10.1002/joc.3758, http://dx.doi.org/10.1002/joc.3758, 2014.

Mäkelä, J., Susiluoto, J., Markkanen, T., Aurela, M., Järvinen, H., Mammarella, I., Hagemann, S., and Aalto, T.: Constraining ecosystem model with adaptive Metropolis algorithm using boreal forest site eddy covariance measurements, Nonlinear Processes in Geophysics, 23, 447–465, doi:10.5194/npg-23-447-2016, http://www.nonlin-processes-geophys.net/23/447/2016/, 2016.

Mammarella, I., Peltola, O., Nordbo, A., Järvi, L., and Rannik, U.: Quantifying the uncertainty of eddy covariance fluxes due to the use of different software packages and combinations of processing steps in two contrasting ecosystems, Atmospheric Measurement Techniques, 9, 4915–4933, doi:10.5194/amt-9-4915-2016, http://www.atmos-meas-tech.net/9/4915/2016/, 2016.

Mastepanov, M., Sigsgaard, C., Tagesson, T., Ström, L., Tamstorf, M. P., Lund, M., and Christensen, T. R.: Revisiting factors controlling methane emissions from high-Arctic tundra, Biogeosciences, 10, 5139–5158, doi:10.5194/bg-10-5139-2013, https://www.biogeosciences.net/10/5139/2013/, 2013.

Melton, J. R., Wania, R., Hodson, E. L., Poulter, B., Ringeval, B., Spahni, R., Bohn, T., Avis, C. A., Beerling, D. J., Chen, G., Eliseev, A. V., Denisov, S. N., Hopcroft, P. O., Lettenmaier, D. P., Riley, W. J., Singarayer, J. S., Subin, Z. M., Tian, H., Zürcher, S., Brovkin, V., van Bodegom, P. M., Kleinen, T., Yu, Z. C., and Kaplan, J. O.: Present state of global wetland extent and wetland methane modelling: conclusions from a model inter-comparison project (WETCHIMP), Biogeosciences, 10, 753–788, doi:10.5194/bg-10-753-2013, https://www.biogeosciences.net/10/753/2013/, 2013.

Müller, J., Paudel, R., Shoemaker, C. A., Woodbury, J., Wang, Y., and Mahowald, N.: CH_4 parameter estimation in CLM4.5bgc using surrogate global optimization, Geoscientific Model Development, 8, 3285–3310, doi:10.5194/gmd-8-3285-2015, http://www.geosci-model-dev.net/8/3285/2015/, 2015.

Nedwell, D. B. and Watson, A.: CH4 production, oxidation and emission in a U.K. ombrotrophic peat bog: Influence of SO42- from acid rain, Soil Biology and Biochemistry, 27, 893 – 903, doi:http://dx.doi.org/10.1016/0038-0717(95)00018-A, http://www.sciencedirect.com/science/article/pii/003807179500018A, 1995.

Nilsson, M. and Öquist, M.: Partitioning Litter Mass Loss into Carbon Dioxide and Methane in Peatland Ecosystems, pp. 131–144, American Geophysical Union, doi:10.1029/2008GM000819, http://dx.doi.org/10.1029/2008GM000819, 2013.

Petrescu, A. M. R., Lohila, A., Tuovinen, J.-P., Baldocchi, D. D., Desai, A. R., Roulet, N. T., Vesala, T., Dolman, A. J., Oechel, W. C., Marcolla, B., Friborg, T., Rinne, J., Matthes, J. H., Merbold, L., Meijide, A., Kiely, G., Sottocornola, M., Sachs, T., Zona, D., Varlagin, A., Lai, D. Y. F., Veenendaal, E., Parmentier, F.-J. W., Skiba, U., Lund, M., Hensen, A., van Huissteden, J., Flanagan, L. B., Shurpali, N. J., Grünwald, T., Humphreys, E. R., Jackowicz-Korczyński, M., Aurela, M. A., Laurila, T., Grüning, C., Corradi, C. A. R., Schrier-Uijl, A. P., Christensen, T. R., Tamstorf, M. P., Mastepanov, M., Martikainen, P. J., Verma, S. B., Bernhofer, C., and Cescatti, A.: The uncertain climate footprint of wetlands under human pressure, Proceedings of the National Academy of Sciences, 112, 4594–4599, doi:10.1073/pnas.1416267112, http://www.pnas.org/content/112/15/4594.abstract, 2015.

Powell, M. J. D.: The BOBYQA algorithm for bound constrained optimization without derivatives, Tech. rep., 2009.

Prather, M. J., Holmes, C. D., and Hsu, J.: Reactive greenhouse gas scenarios: Systematic exploration of uncertainties and the role of atmospheric chemistry, Geophysical Research Letters, 39, n/a–n/a, doi:10.1029/2012GL051440, http://dx.doi.org/10.1029/2012GL051440, l09803, 2012.

Raivonen, M., Mäkiranta, P., Lohila, A., Juutinen, S., Vesala, T., and Tuittila, E.-S.: A simple {CO2} exchange model simulates the seasonal leaf area development of peatland sedges, Ecological Modelling, 314, 32 – 43, doi:http://dx.doi.org/10.1016/j.ecolmodel.2015.07.008, http://www.sciencedirect.com/science/article/pii/S0304380015003142, 2015.

Raivonen, M., Smolander, S., Backman, L., Susiluoto, J., Aalto, T., Markkanen, T., Mäkelä, J., Rinne, J., Peltola, O., Aurela, M., Lohila, A., Tomasic, M., Li, X., Larmola, T., Juutinen, S., Tuittila, E.-S., Heimann, M., Sevanto, S., Kleinen, T., Brovkin, V., and Vesala, T.: HIMMELI v1.0: HelsinkI Model of MEthane buiLd-up and emIssion for peatlands, Geoscientific Model Development, 10, 4665–4691, doi:10.5194/gmd-10-4665-2017, https://www.geosci-model-dev.net/10/4665/2017/, 2017.

Rezanezhad, F., Price, J. S., Quinton, W. L., Lennartz, B., Milojevic, T., and Cappellen, P. V.: Structure of peat soils and implications for water storage, flow and solute transport: A review update for geochemists, Chemical Geology, 429, 75 – 84, doi:http://dx.doi.org/10.1016/j.chemgeo.2016.03.010, http://www.sciencedirect.com/science/article/pii/S0009254116301243, 2016.

Ricciuto, D. M., Davis, K. J., and Keller, K.: A Bayesian calibration of a simple carbon cycle model: The role of observations in estimating and reducing uncertainty, Global Biogeochemical Cycles, 22, n/a–n/a, doi:10.1029/2006GB002908, http://dx.doi.org/10.1029/2006GB002908, gB2030, 2008.

Richardson, A. D., Hollinger, D. Y., Burba, G. G., Davis, K. J., Flanagan, L. B., Katul, G. G., Munger, J. W., Ricciuto, D. M., Stoy, P. C., Suyker, A. E., Verma, S. B., and Wofsy, S. C.: A multi-site analysis of random error in tower-based measurements of carbon and energy fluxes, Agricultural and Forest Meteorology, 136, 1 – 18, doi:http://dx.doi.org/10.1016/j.agrformet.2006.01.007, http://www.sciencedirect.com/science/article/pii/S0168192306000281, 2006.

Riley, W. J., Subin, Z. M., Lawrence, D. M., Swenson, S. C., Torn, M. S., Meng, L., Mahowald, N. M., and Hess, P.: Barriers to predicting changes in global terrestrial methane fluxes: analyses using CLM4Me, a methane biogeochemistry model integrated in CESM, Biogeosciences, 8, 1925–1953, doi:10.5194/bg-8-1925-2011, http://www.biogeosciences.net/8/1925/2011/, 2011.

Rinne, J., Riutta, T., Pihlatie, M., Aurela, M., Haapanala, S., Tuovinen, J.-P., Tuittila, E.-S., and Vesala, T.: Annual cycle of methane emission from a boreal fen measured by the eddy covariance technique, Tellus B, 59, 449–457, doi:10.1111/j.1600-0889.2007.00261.x, http://dx.doi.org/10.1111/j.1600-0889.2007.00261.x, 2007.

Riutta, T., Laine, J., Aurela, M., Rinne, J., Vesala, T., Laurila, T., Haapanala, S., Pihlatie, M., and Tuittila, E.-S.: Spatial variation in plant community functions regulates carbon gas dynamics in a boreal fen ecosystem, Tellus B, 59, 838–852, doi:10.1111/j.1600-0889.2007.00302.x, http://dx.doi.org/10.1111/j.1600-0889.2007.00302.x, 2007a.

Riutta, T., Laine, J., and Tuittila, E.-S.: Sensitivity of CO2 Exchange of Fen Ecosystem Components to Water Level Variation, Ecosystems, 10, 718–733, doi:10.1007/s10021-007-9046-7, http://dx.doi.org/10.1007/s10021-007-9046-7, 2007b.

Roberts, G. O., Gelman, A., and Gilks, W. R.: Weak convergence and optimal scaling of random walk Metropolis algorithms, Ann. Appl. Probab., 7, 110–120, doi:10.1214/aoap/1034625254, http://dx.doi.org/10.1214/aoap/1034625254, 1997.

Ruosteenoja, K., Jylhä, K., and Kämäräinen, M.: Climate Projections for Finland Under the RCP Forcing Scenarios, Geophysica, 51, 17–50, 2016.

Saarinen, T.: Biomass and production of two vascular plants in a boreal mesotrophic fen, Canadian Journal of Botany, 74, 934–938, doi:10.1139/b96-116, http://dx.doi.org/10.1139/b96-116, 1996.

Saarinen, T.: Demography of Carex rostrata in boreal mesotrophic fen: shoot dynamics and biomass development, Ann. Bot. Fennici, pp. 203–209, 1998.

Sanso, B., Forest, C., and Zantedeschi, D.: Inferring Climate System Properties Using a Computer Model, Tech. rep., 2007.

Saunois, M., Bousquet, P., Poulter, B., Peregon, A., Ciais, P., Canadell, J. G., Dlugokencky, E. J., Etiope, G., Bastviken, D., Houweling, S., Janssens-Maenhout, G., Tubiello, F. N., Castaldi, S., Jackson, R. B., Alexe, M., Arora, V. K., Beerling, D. J., Bergamaschi, P., Blake, D. R., Brailsford, G., Brovkin, V., Bruhwiler, L., Crevoisier, C., Crill, P., Covey, K., Curry, C., Frankenberg, C., Gedney, N., Höglund-Isaksson, L., Ishizawa, M., Ito, A., Joos, F., Kim, H.-S., Kleinen, T., Krummel, P., Lamarque, J.-F., Langenfelds, R., Locatelli, R., Machida, T., Maksyutov, S., McDonald, K. C., Marshall, J., Melton, J. R., Morino, I., Naik, V., O'Doherty, S., Parmentier, F.-J. W., Patra, P. K., Peng, C., Peng, S., Peters, G. P., Pison, I., Prigent, C., Prinn, R., Ramonet, M., Riley, W. J., Saito, M., Santini, M., Schroeder, R., Simpson, I. J., Spahni, R., Steele, P., Takizawa, A., Thornton, B. F., Tian, H., Tohjima, Y., Viovy, N., Voulgarakis, A., van Weele, M., van der Werf, G. R., Weiss, R., Wiedinmyer, C., Wilton, D. J., Wiltshire, A., Worthy, D., Wunch, D., Xu, X., Yoshida, Y., Zhang, B.,

Zhang, Z., and Zhu, Q.: The global methane budget 2000–2012, Earth System Science Data, 8, 697–751, doi:10.5194/essd-8-697-2016, http://www.earth-syst-sci-data.net/8/697/2016/, 2016.

Schuldt, R. J., Brovkin, V., Kleinen, T., and Winderlich, J.: Modelling Holocene carbon accumulation and methane emissions of boreal wetlands – an Earth system model approach, Biogeosciences, p. 1659–1674, 2013.

Segers, R.: Methane production and methane consumption: a review of processes underlying wetland methane fluxes, Biogeochemistry, 41, 23–51, doi:10.1023/A:1005929032764, http://dx.doi.org/10.1023/A:1005929032764, 1998.

Sriskantharajah, S., Fisher, R. E., Lowry, D., Aalto, T., Hatakka, J., Aurela, M., Laurila, T., Lohila, A., Kuitunen, E., and Nisbet, E. G.: Stable carbon isotope signatures of methane from a Finnish subarctic wetland, Tellus B: Chemical and Physical Meteorology, 64, 18 818, doi:10.3402/tellusb.v64i0.18818, https://doi.org/10.3402/tellusb.v64i0.18818, 2012.

Stephen, K., Arah, J., Thomas, K., Benstead, J., and Lloyd, D.: Gas diffusion coefficient profile in peat determined by modelling mass spectrometric data: implications for gas phase distribution, Soil Biology and Biochemistry, 30, 429 – 431, doi:http://dx.doi.org/10.1016/S0038-0717(97)00118-1, http://www.sciencedirect.com/science/article/pii/S0038071797001181, 1998.

Szafranek-Nakonieczna, A. and Stepniewska, Z.: Aerobic and anaerobic respiration in profiles of Polesie Lubelskie peatlands, International Agrophysics, 28, 219–229, doi:doi: 10.2478/intag-2014-0011, 2014.

Tang, J., Zhuang, Q., Shannon, R. D., and White, J. R.: Quantifying wetland methane emissions with process-based models of different complexities, Biogeosciences, 7, 3817–3837, doi:10.5194/bg-7-3817-2010, http://www.biogeosciences.net/7/3817/2010/, 2010.

van Huissteden, J., Petrescu, A. M. R., Hendriks, D. M. D., and Rebel, K. T.: Sensitivity analysis of a wetland methane emission model based on temperate and arctic wetland sites, Biogeosciences, 6, 3035–3051, doi:10.5194/bg-6-3035-2009, http://www.biogeosciences.net/6/3035/2009/, 2009.

Vile, D., Garnier, E., Shipley, B., Laurent, G., Navas, M.-L., Roumet, C., Lavorel, S., Díaz, S., Hodgson, J. G., Lloret, F., Midgley, G. F., Poorter, H., Rutherford, M. c., Wilson, P. J., and Wright, I. J.: Specific Leaf Area and Dry Matter Content Estimate Thickness in Laminar Leaves, Annals of Botany, 96, 1129, doi:10.1093/aob/mci264, +http://dx.doi.org/10.1093/aob/mci264, 2005.

Walker, T. S., Bais, H. P., Grotewold, E., and Vivanco, J. M.: Root Exudation and Rhizosphere Biology, Plant Physiology, 132, 44–51, doi:10.1104/pp.102.019661, http://www.plantphysiol.org/content/132/1/44.short, 2003.

Walter, B. P. and Heimann, M.: A process-based, climate-sensitive model to derive methane emissions from natural wetlands: Application to five wetland sites, sensitivity to model parameters, and climate, Global Biogeochemical Cycles, 14, 745–765, doi:10.1029/1999GB001204, http://dx.doi.org/10.1029/1999GB001204, 2000.

Wania, R.: Modelling northern peatland land surface processes, vegetation dynamics and methane emissions, Ph.D. thesis, University of Bristol, 2007.

Wania, R., Ross, I., and Prentice, I. C.: Implementation and evaluation of a new methane model within a dynamic global vegetation model: LPJ-WHyMe v1.3.1, Geoscientific Model Development, 3, 565–584, 2010.

Watson, A., Stephen, K. D., Nedwell, D. B., and Arah, J. R.: Oxidation of Methane in Peat: Kinetics of CH4 and O2 Removal and the Role of Plant Roots, Soil Biol. Biochem., 29, 1997.

Whiting, G. J. and Chanton, J. P.: Primary production control of methane emission from wetlands, Nature, 364, 794–795, doi:10.1038/364794a0, http://dx.doi.org/10.1038/364794a0, 1993.

Wilson, D., Alm, J., Riutta, T., Laine, J., Byrne, K. A., Farrell, E. P., and Tuittila, E.-S.: A high resolution green area index for modelling the seasonal dynamics of CO2 exchange in peatland vascular plant communities, Plant Ecology, 190, 37–51, doi:10.1007/s11258-006-9189-1, http://dx.doi.org/10.1007/s11258-006-9189-1, 2007.

Zhu, Q., Liu, J., Peng, C., Chen, H., Fang, X., Jiang, H., Yang, G., Zhu, D., Wang, W., and Zhou, X.: Modelling methane emissions from natural wetlands by development and application of the TRIPLEX-GHG model, Geoscientific Model Development, 7, 981–999, doi:10.5194/gmd-7-981-2014, http://www.geosci-model-dev.net/7/981/2014/, 2014.

Table 1. Description of the data used

Data	Description	Usage	Units	Source	Comments
LAI	leaf area index	input	-	modeled	Gaussian curve to approximate the seasonal cycle
WTD	water table depth	input	m	measured	gap-filled at various times
NPP	net primary prod.	input	mol m^{-2} s^{-1}	modeled	generated by a separate NPP model
T_{soil}	soil temperature	input	°C	measured	interpolated from fewer observation depths
CH_4	CH_4 flux	objective function	mol m^{-2} s^{-1}	measured	used in the objective function formulation
CO_2	CO_2 flux	objective function	mol m^{-2} s^{-1}	measured	used in the objective function formulation

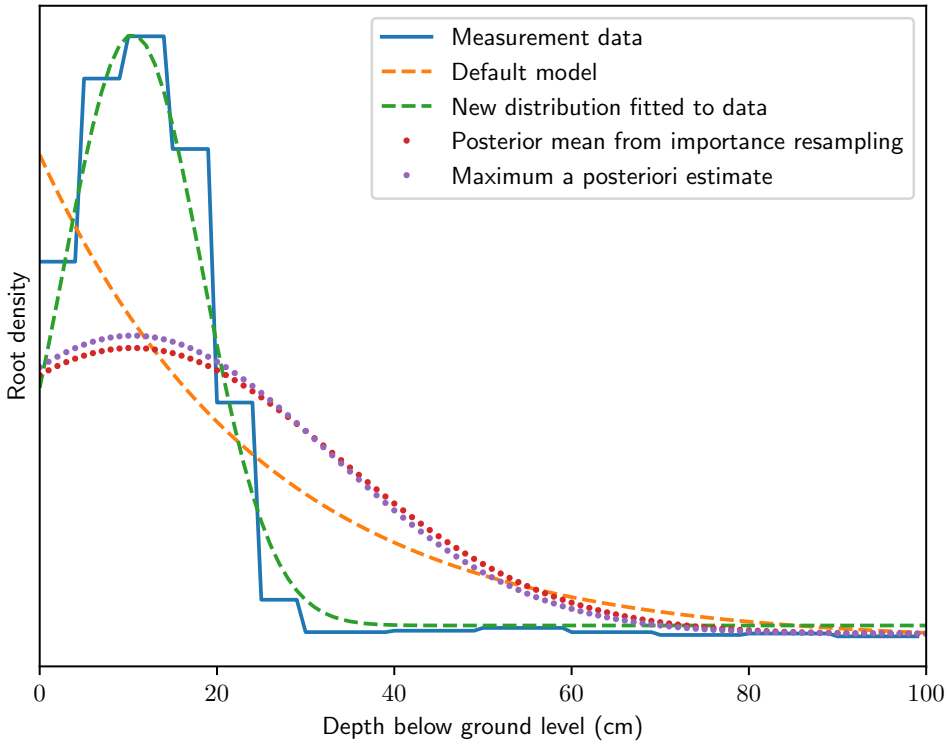

Figure 1. The different root distribution descriptions. The original description is shown as the decaying exponential, and the graph with discrete steps shows measurement data from Saarinen (1996). The new root distribution curve with optimized parameters are shown along with the curves resulting from the MCMC optimization. The original distribution gives more root mass to depths of 50-80cm, than the MCMC-optimized curves of the new root distribution. All curves are normalized to the same total root mass.

Table 2. Parameters that were not calibrated. Based on an initial sensitivity analysis, the Michaelis-Menten parameters K were not constrained by the data enough strongly and consistently to include them in the optimization. The same applies for the ebullition half-life, which is understandable given the temporal resolution of the observed data. The peat porosity was dropped from optimization in favor of the diffusivity parameters $f_{D,w}$ and $f_{D,a}$, and the specific leaf area was not chosen for optimization since the optimized parameters τ (m m^{-1}) and ρ (m^2 kg^{-1}) are already part of the equation 22 where SLA appears. The parameter $g_{CH_4}^{Q_{10}}$ was left out in favor of parameter τ_{cato}, despite their functions regarding CO_2 being different, but trusting the prior value.

Parameter	Equation	Value	Units	Description	Source
$g_{CH_4}^{Q_{10}}$	16	0.4	-	peat decay to CH_4 fraction	Schuldt et al. (2013)
K_R	19	0.022	mol m^{-3}	Michaelis-Menten coeff.	Nedwell and Watson (1995)
K_{CH_4}	20	0.044	mol m^{-3}	Michaelis-Menten coeff.	Nedwell and Watson (1995)
K_{O_2}	20	0.033	mol m^{-3}	Michaelis-Menten coeff.	Nedwell and Watson (1995)
SLA	22	23	m^{2}kg^{-1}	specific leaf area	Vile et al. (2005)
k	23	$\log(2)/1800$	s^{-1}	ebullition rate constant	-
σ	23	0.5	-	peat porosity	Rezanezhad et al. (2016)

	Low	High	Units	Prior μ	Prior σ	Source
$f_{D,a}$	0.01	1.0	-	0.8	0.2	(Raivonen et al., 2017)
$f_{D,w}$	0.01	1.0	-	0.8	0.2	(Raivonen et al., 2017)
V_{R0}	2×10^{-6}	1×10^{-4}	mol m^{-3} s^{-1}	1×10^{-5}	2×10^{-5}	(Nedwell and Watson, 1995; Watson et al., 1997)
V_{O0}	2×10^{-6}	3×10^{-4}	mol m^{-3} s^{-1}	1×10^{-5}	2×10^{-5}	Same as (Raivonen et al., 2017), also (Segers, 1998),
λ_{root}	0.01	0.4	m	0.125	0.05	Fitted to data in (Saarinen, 1996)
τ	1.0	5.0	m m^{-1}	1.5	0.2	(Stephen et al., 1998)
ρ	0.05	0.4	m^2 kg^{-1}	0.085	0.0425	(Stephen et al., 1998)
τ_{exu}	3	30	days	14	2.5	(Wania, 2007)
τ_{cato}	1000	30000	years	-	-	Flat prior
ΔE_R	5000	200000	J mol^{-1}	50000	5000	(Nedwell and Watson, 1995)
ΔE_{oxid}	5000	200000	J mol^{-1}	50000	5000	(Nedwell and Watson, 1995)
$f_{CH_4}^{\mathrm{exu}}$	0.5	0.77	-	0.635	0.06	(Nilsson and Öquist, 2013)
Q_{10}	1.7	16.0	-	5.9	0.5*	(Juottonen, 2008; Gedney et al., 2004; Bergman et al., 2000)
ζ_{exu}	0.01	0.99	-	0.5	0.2*	(Walker et al., 2003)

Table 3. Parameter limits and prior distribution parameters. The priors are truncated Gaussian, with mean values μ and standard deviations σ, truncated at the values in the columns *low* and *high*. *For importance resampling, the hierarchical modeled parameters' (Q_{10} (-) and ζ_{exu} (-)) priors were relaxed by a factor of three, to allow for a more data-constrained resampling, and to accommodate the low values of Q_{10} reported by Szafranek-Nakonieczna and Stepniewska (2014). Note that the values of the prior for these two parameters were sampled at each iteration with Gibbs sampling.

.

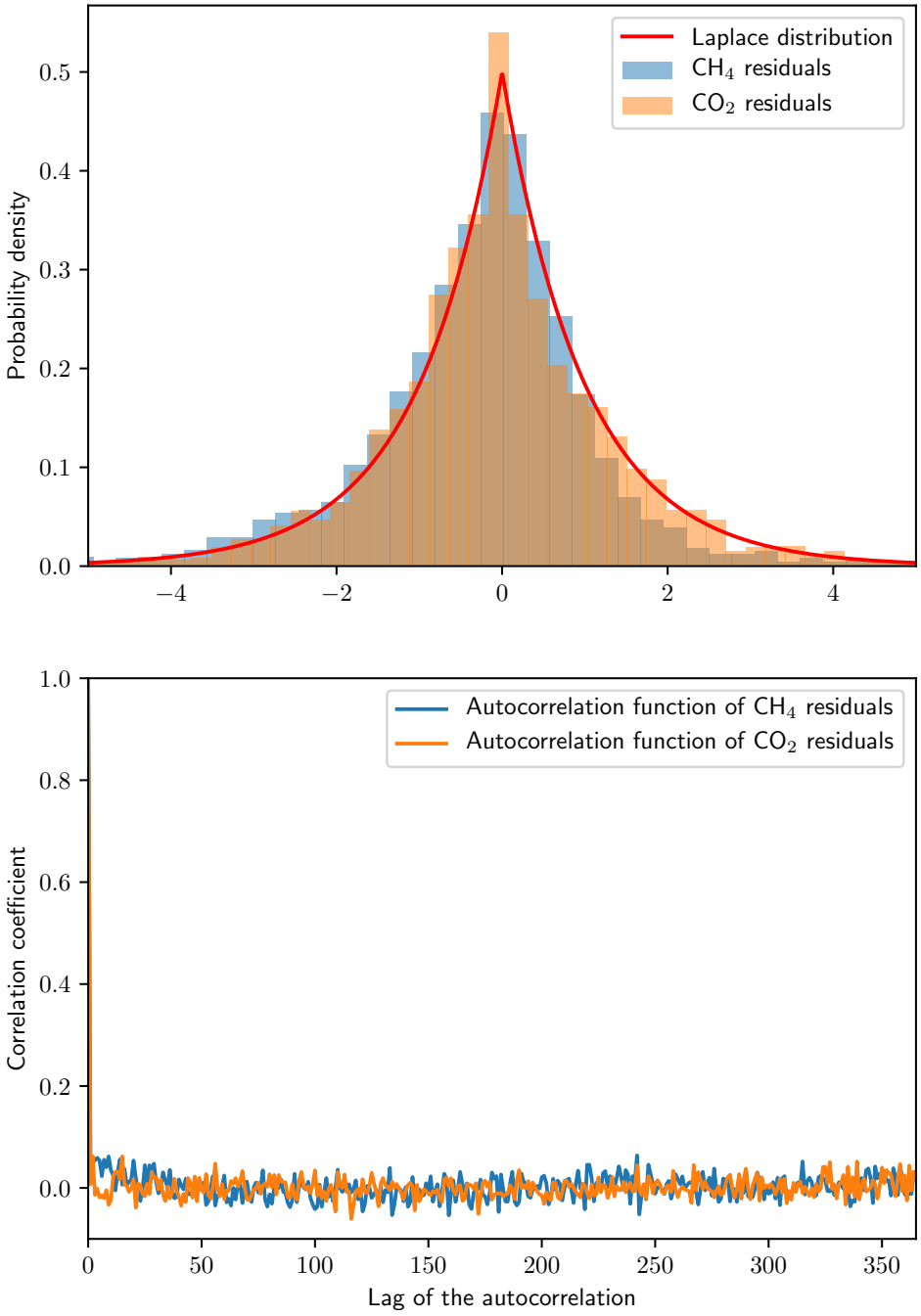

Figure 2. Residual histograms and autocorrelation functions of the error terms ϵ_t in the objective function, Eq. 24, show that neither the CO_2 nor the CH_4 residuals are autocorrelated and that they closely follow the Laplace-distribution. The results shown are for the residuals from the posterior mean estimate.

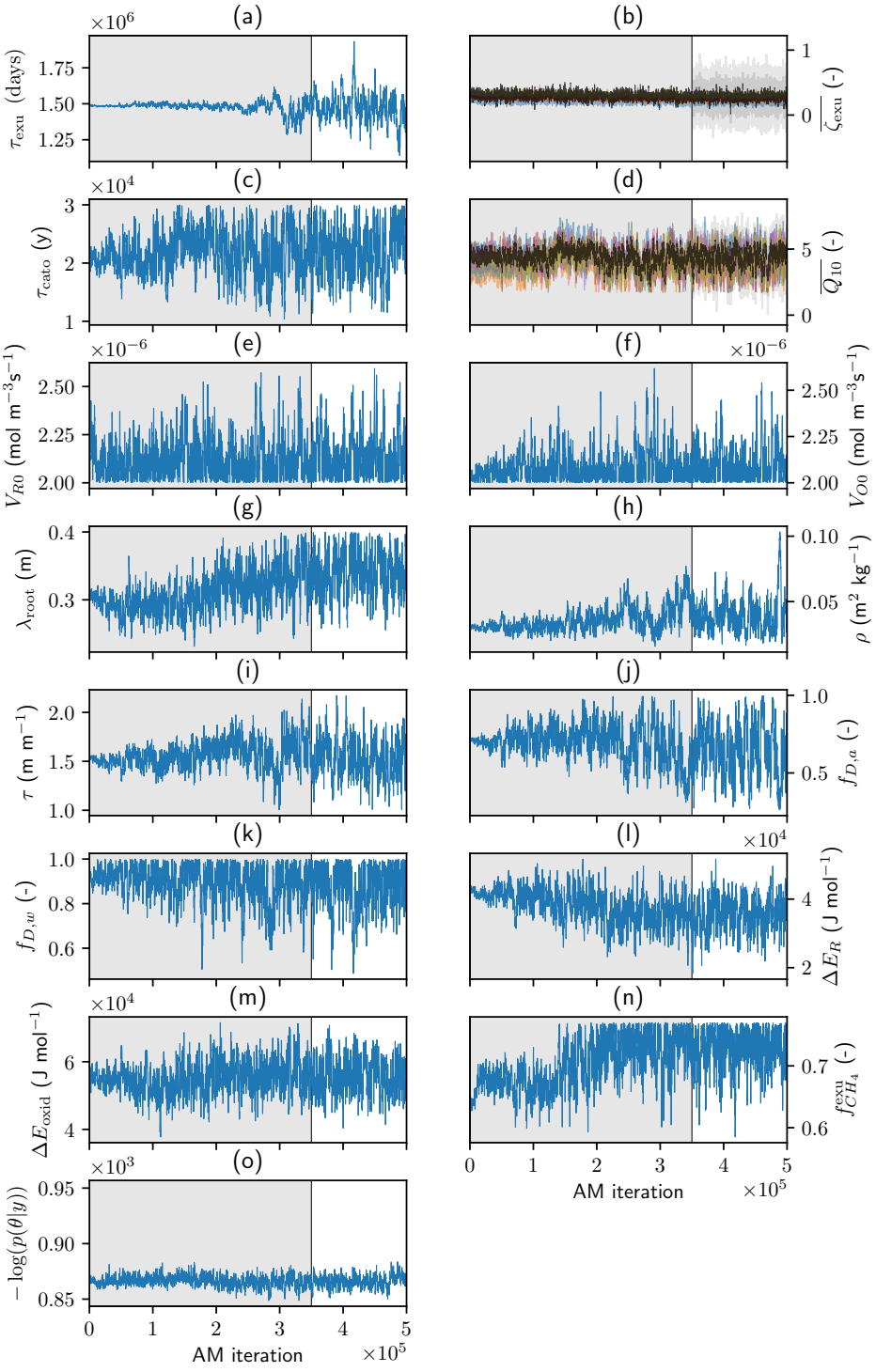

Figure 3. MCMC chains showing a thinned sample of the half million values in the chain. The first 70% was discarded for the analyses as warm-up and is grayed out in the figures. The hierarchical parameters in (b) and (d) show the mean value in the middle as a black mass, and the colorful surroundings are the values of the parameters for the individual years. The last figure (o) shows the value of the objective function.

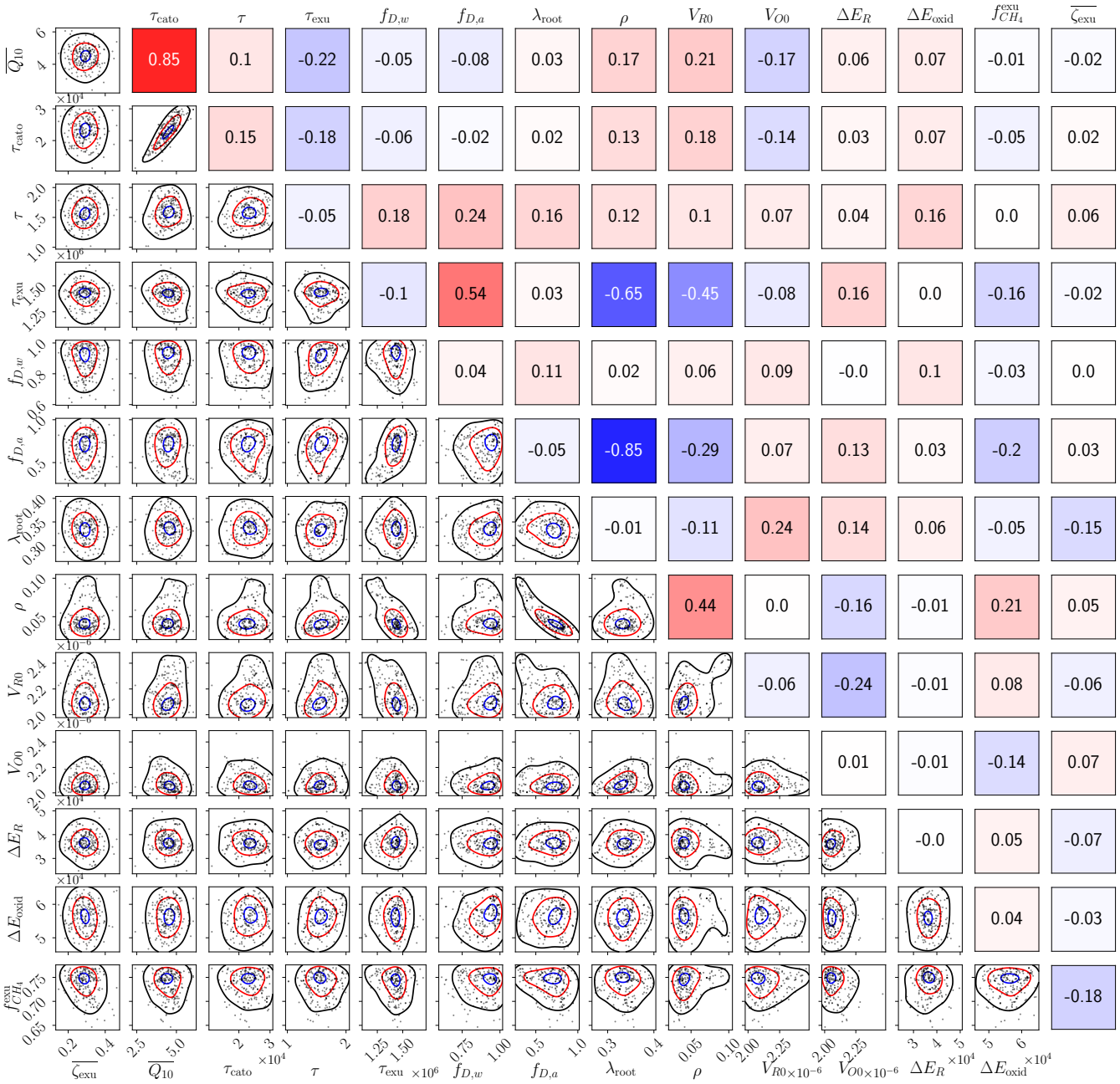

Figure 4. Posterior distributions of the parameters from the importance sampling. The two-dimensional marginal distributions of the posterior distribution is shown in the triangle on the lower left (labels on the left and at the bottom), and the correlations between parameters are shown in the upper triangle on the right (labels on the left and at the top). The images in the lower left triangle show the 90% (black) 50% (red), and 10% (blue) contours, and a points from a random sample of the posterior (black dots). On the upper right, each plot shows correlation coefficients between parameters, color-coded to show negative correlations in blue and positive in red. The units are listed in Table 4.

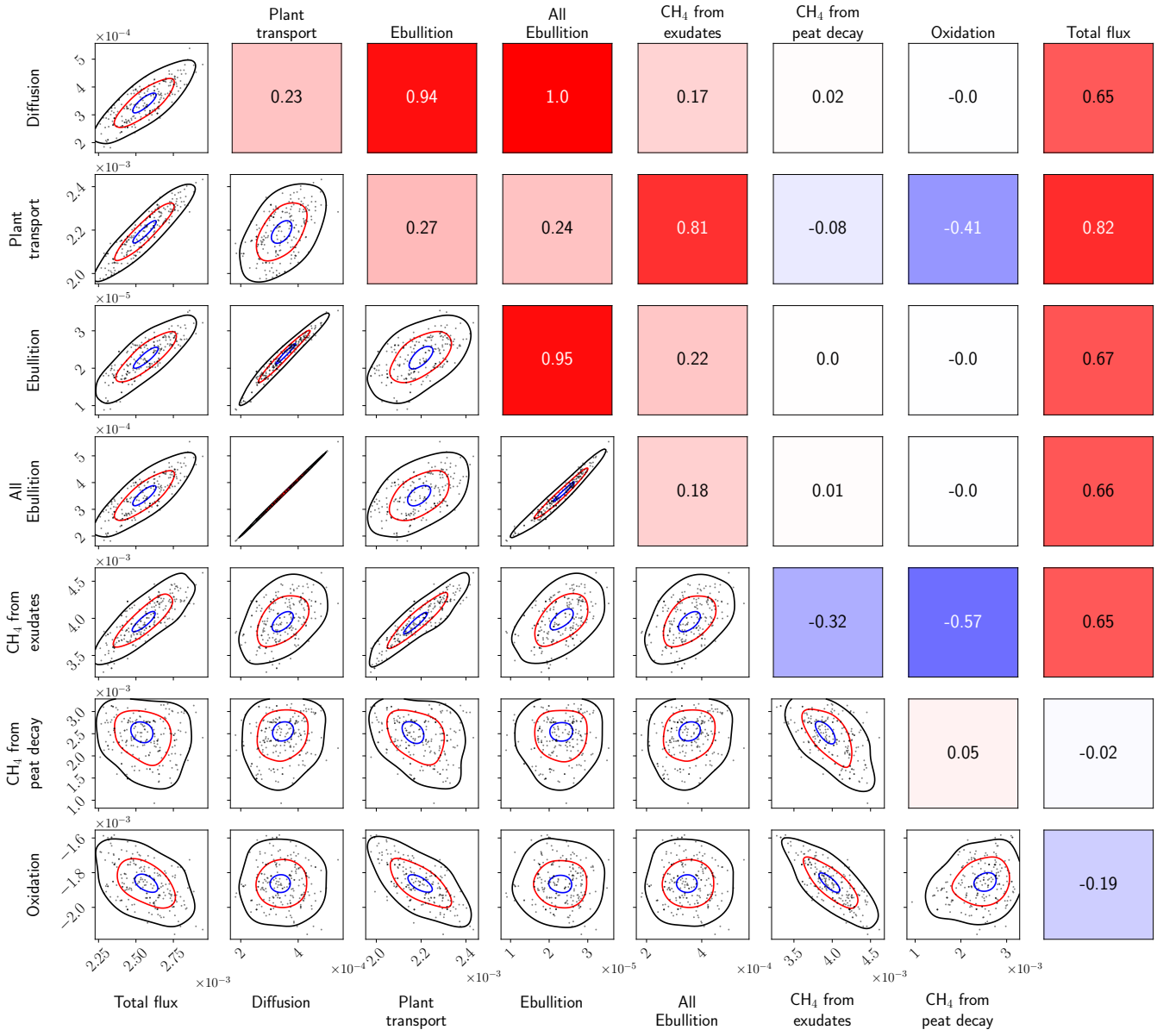

Figure 5. Posterior distributions and correlations of the annual means of the output from the modeled processes for the year 2012. The dynamics for the other years are mostly similar but the strengths of the correlations vary somewhat. The results shown are based on 1000 random samples from the parameter posterior distribution. The two-dimensional marginal distributions in the triangle on the lower left have their labels on the left and at the bottom, and the correlations between the processes in the upper triangle on the right have their labels on the left and on the top. The images in the lower left triangle show the 90% (black) 50% (red), and 10% (blue) contours. The all ebullition and diffusion fluxes correlate almost fully showing that the "diffusion"-flux has a strong contribution from underground ebullition.

Table 4. Parameter values obtained in the optimization of the sqHIMMELI model with importance resampling. The maximum a posterior, posterior mean, non-hierarchical mean (mean values used for hierarchically varying parameters), and values from Raivonen et al. (2017) are shown. The horizontal line in the middle separates the hierarchically optimized parameters (including their priors) from the others.

Parameter	MAP	Posterior mean	Non-hier. mean	Default
$\tau_{\mathrm{cato}}(\times 10^4$ y)	2.872	2.269	2.269	3.0
τ (m m^{-1})	1.462	1.581	1.581	1.5
$\tau_{\mathrm{exu}}(\times 10^6 s)$	1.187	1.411	1.411	1.21
$f_{D,w}$ (-)	0.866	0.887	0.887	0.8
$f_{D,a}$ (-)	0.427	0.65	0.65	0.8
λ_{root} (m)	0.314	0.333	0.333	0.252
ρ (m^2 kg^{-1})	0.081	0.049	0.049	0.085
$V_{R0}(\times 10^{-6}$ mol m^{-3} s^{-1})	2.366	2.153	2.153	10.0
$V_{O0}(\times 10^{-6}$ mol m^{-3} s^{-1})	2.013	2.09	2.09	10.0
$\Delta E_R(\times 10^4$ J mol^{-1})	3.478	3.647	3.647	5.0
$\Delta E_{\mathrm{oxid}}(\times 10^4$ J mol^{-1})	5.358	5.575	5.575	5.0
$f_{CH_4}^{\mathrm{exu}}$ (-)	0.729	0.736	0.736	0.5
$\overline{\zeta_{\mathrm{exu}}}$ (-)	0.343	0.292	-	-
$\zeta_{\mathrm{exu}}^{\mathrm{std}}$ (-)	0.128	0.157	-	-
$\overline{Q_{10}}$ (-)	5.721	4.425	-	-
Q_{10}^{std} (-)	0.587	0.616	-	-
$\zeta_{\mathrm{exu}}^{2006}$ (-)	0.212	0.182	0.292	0.4
$\zeta_{\mathrm{exu}}^{2007}$ (-)	0.251	0.244	0.292	0.4
$\zeta_{\mathrm{exu}}^{2008}$ (-)	0.28	0.276	0.292	0.4
$\zeta_{\mathrm{exu}}^{2009}$ (-)	0.202	0.243	0.292	0.4
$\zeta_{\mathrm{exu}}^{2010}$ (-)	0.34	0.314	0.292	0.4
$\zeta_{\mathrm{exu}}^{2011}$ (-)	0.251	0.258	0.292	0.4
$\zeta_{\mathrm{exu}}^{2012}$ (-)	0.327	0.324	0.292	0.4
$\zeta_{\mathrm{exu}}^{2013}$ (-)	0.368	0.313	0.292	0.4
$\zeta_{\mathrm{exu}}^{2014}$ (-)	0.334	0.323	0.292	0.4
Q_{10}^{2006} (-)	5.946	4.488	4.425	3.5
Q_{10}^{2007} (-)	4.882	3.857	4.425	3.5
Q_{10}^{2008} (-)	4.017	3.684	4.425	3.5
Q_{10}^{2009} (-)	5.469	4.14	4.425	3.5
Q_{10}^{2010} (-)	5.337	4.284	4.425	3.5
Q_{10}^{2011} (-)	6.306	4.305	4.425	3.5
Q_{10}^{2012} (-)	5.377	4.193	4.425	3.5
Q_{10}^{2013} (-)	5.219	4.211	4.425	3.5
Q_{10}^{2014} (-)	6.438	4.332	4.425	3.5
Costfunction value	1205.22	1227.01	-	-

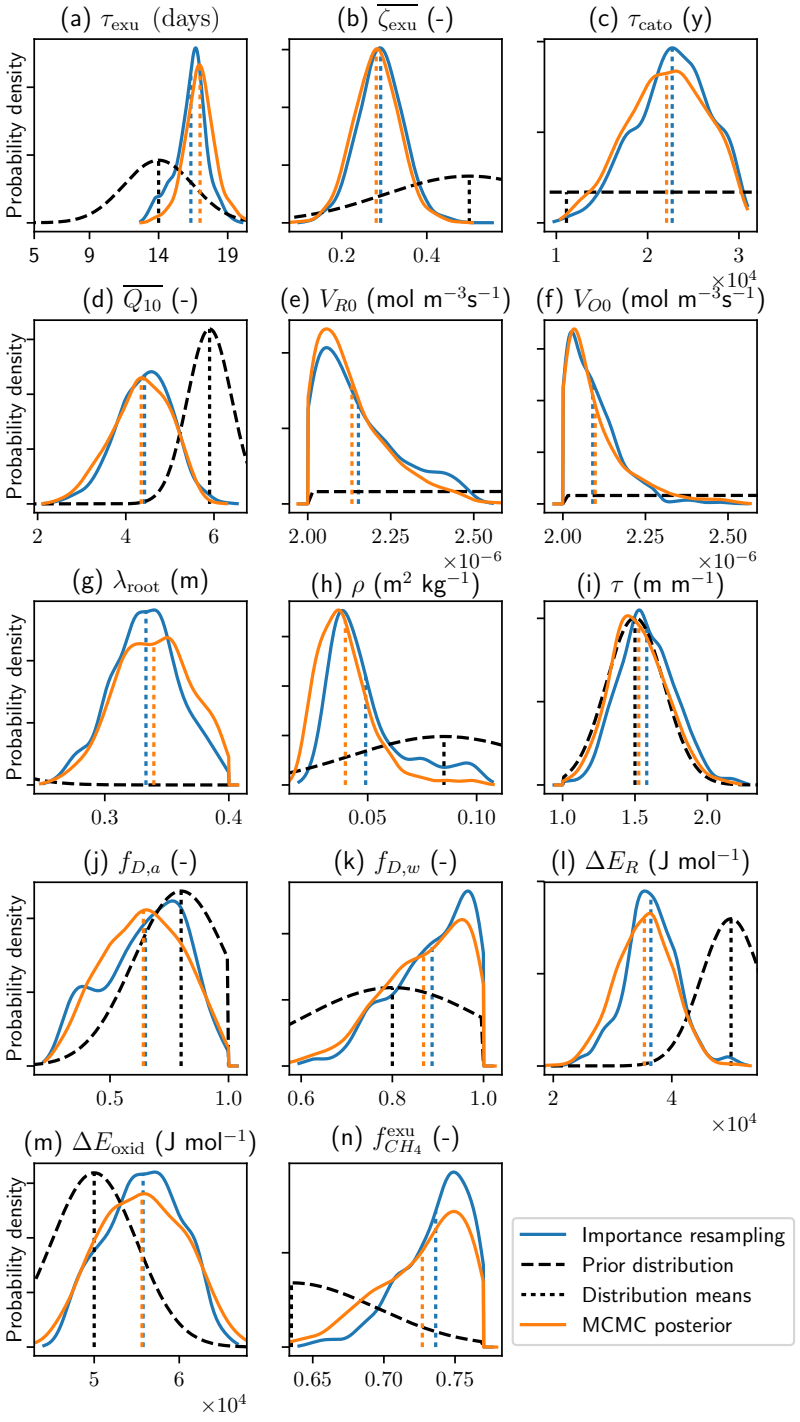

Figure 6. Posterior marginal and prior distributions from MCMC and importance resampling for all parameters: (a-d) and (n) are the production-related, (e-f) and (l-m) the respiration and oxidation related, and (g-k) the gas transport related parameters. The blue and orange curves shown are smoothed slightly using Gaussian kernel estimates for readability. To make these figures, 70% from the start of the MCMC chain was discarded as warm-up (orange line). The dotted vertical lines show the prior mean values and the sample means from both MCMC and importance sampling. For the parameters $\overline{\zeta_{\mathrm{exu}}}$ (b) and $\overline{Q_{10}}$ (d), the prior distribution drawn is the hyperprior.

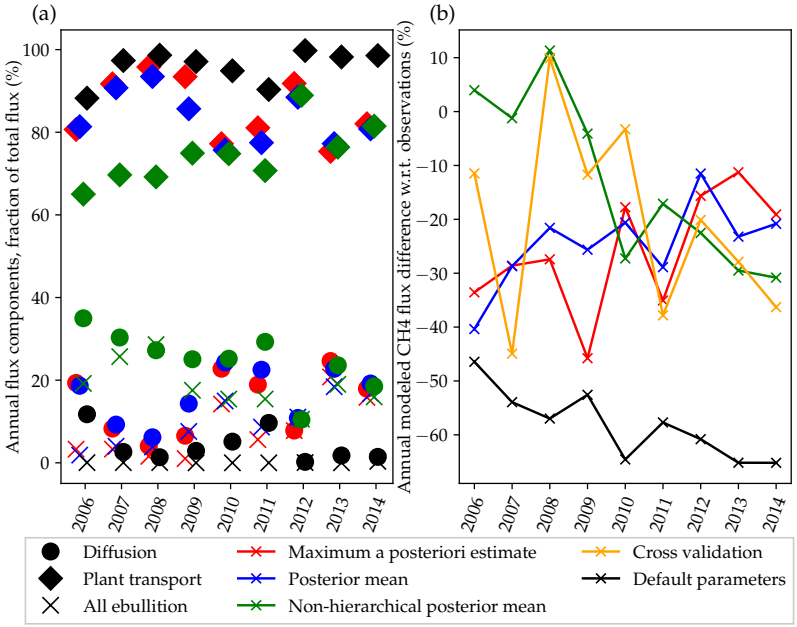

Figure 7. On the left side: proportions of flux components as a function of the year. Diamonds are for plant transport, balls for the diffusion flux, and crosses describe the total ebullition taking place. The figure on the right shows the annual model-observation mismatch in percents for the methane flux, where only residuals from days with observation data available have been taken into account. The data in sub-figure (a) has been spread slightly for readability in the x-axis direction. The orange line in sub-figure (b) represent the results from the cross validation discussed in Sec. 5.6. Note that the optimization target was not to directly fit annual emissions.

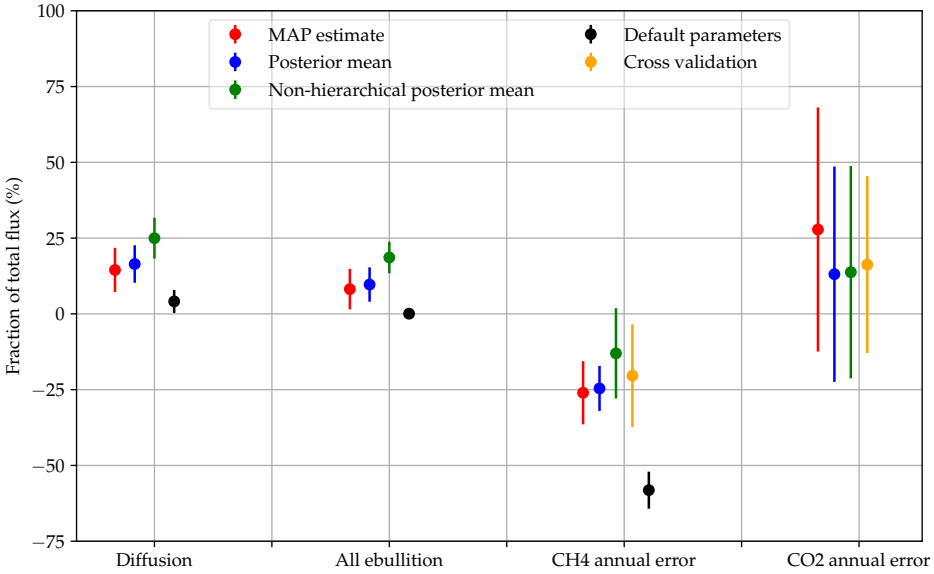

Figure 8. Fractions of the annual diffusive fluxes of the total fluxes. Means and 1-σ error bars are shown. Almost all ebullition takes place when the water table is below the peat surface and hence it is emitted to the atmosphere as part of the diffusion flux. Plant transport is not shown, as it is very close to the complement of the diffusive flux: together these two streams add up to more than 98% of the total flux. Plant transport variation is very close to that of diffusion. On the right side of the figure the average annual errors are shown for the interannual variation of the fluxes. The results of the cross validation of the regression modeling of the hierarchically varying parameters, discussed in Sec. 5.6, are drawn in orange. The "Default" parameters produce carbon dioxide fluxes that are above the upper limit of the chart.

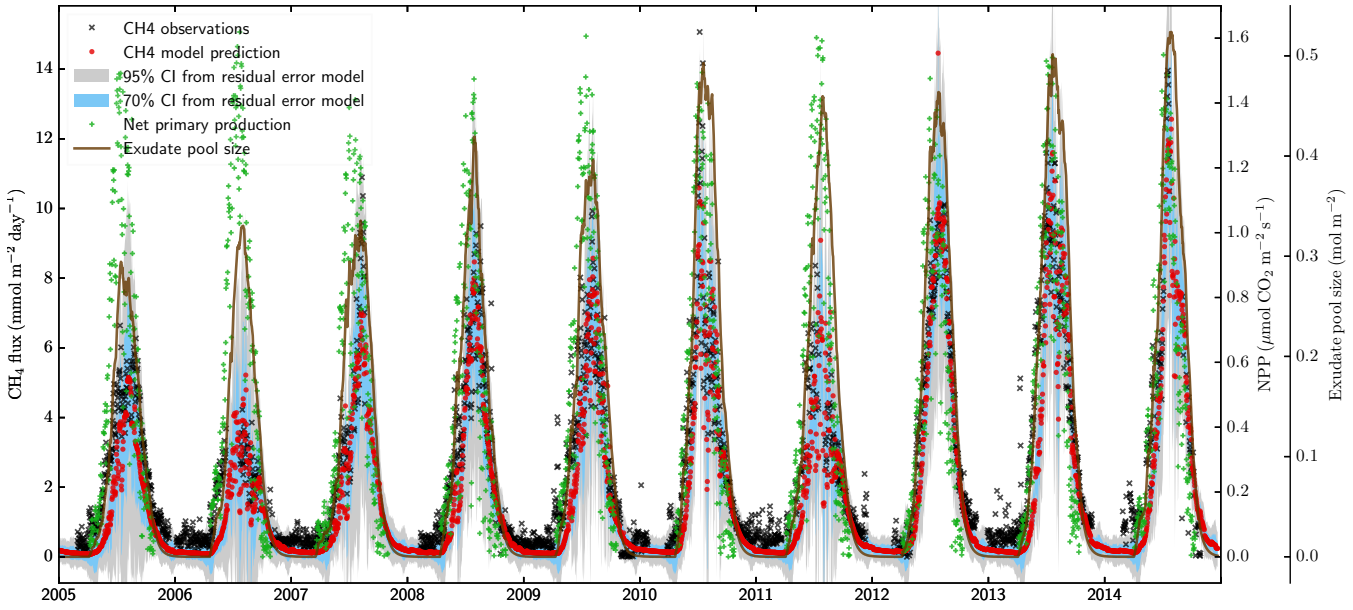

Figure 9. Output CH_4 flux (red dots) with parameters from the posterior mean. Methane observations (black crosses) and predicted fluxes with confidence intervals from ARMA(2,1) modeling of a set of 1000 residual timeseries are shown, as are the input net primary production (green dots) and the exudate pool sizes (brown line). Most of the observations are inside the confidence intervals, but note that the effects of the parameter variations in the posterior are not part of these confidence intervals. The constituents of the total flux are shown in Fig. 12.

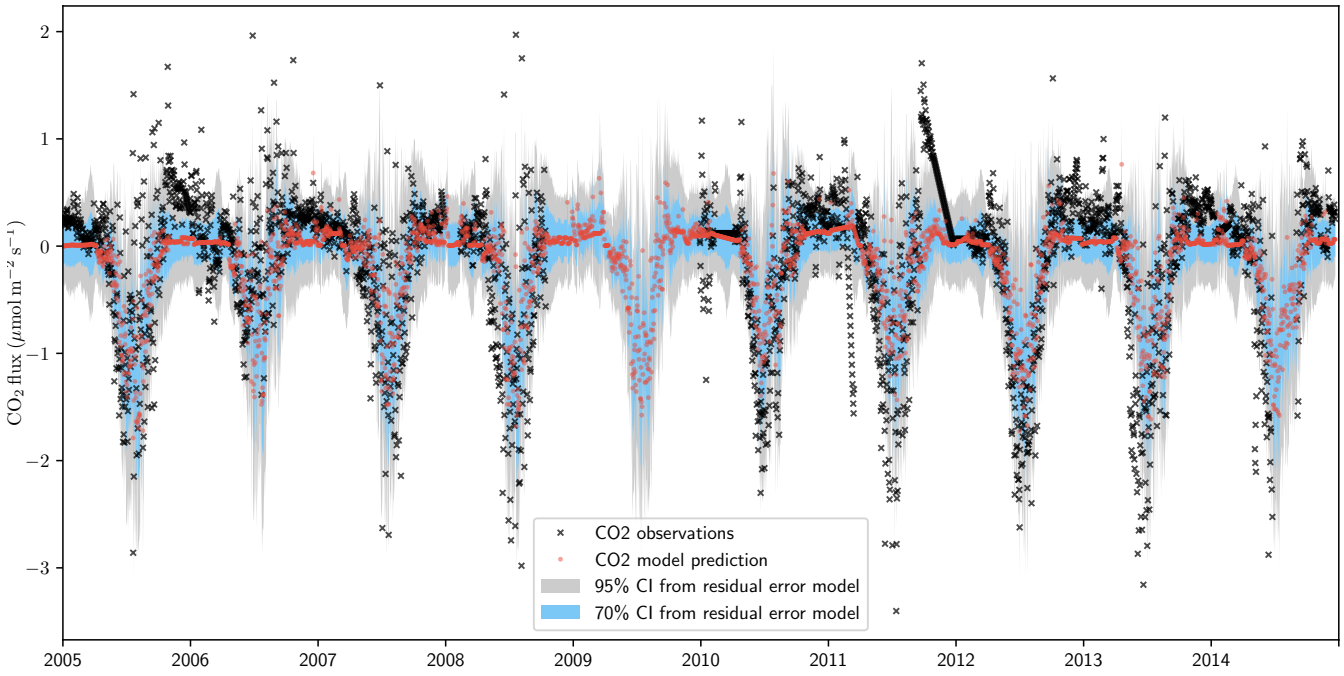

Figure 10. Output CO_2 flux (red dots) with parameters from the posterior mean. Carbon dioxide observations (black crosses) and model predicted fluxes with confidence intervals from the ARMA(2,1) modeling of a set of 1000 residual timeseries are also shown. As with methane, most of the observations are inside the confidence intervals. The parameter variations in the posterior probability distribution are not reflected in these confidence intervals.

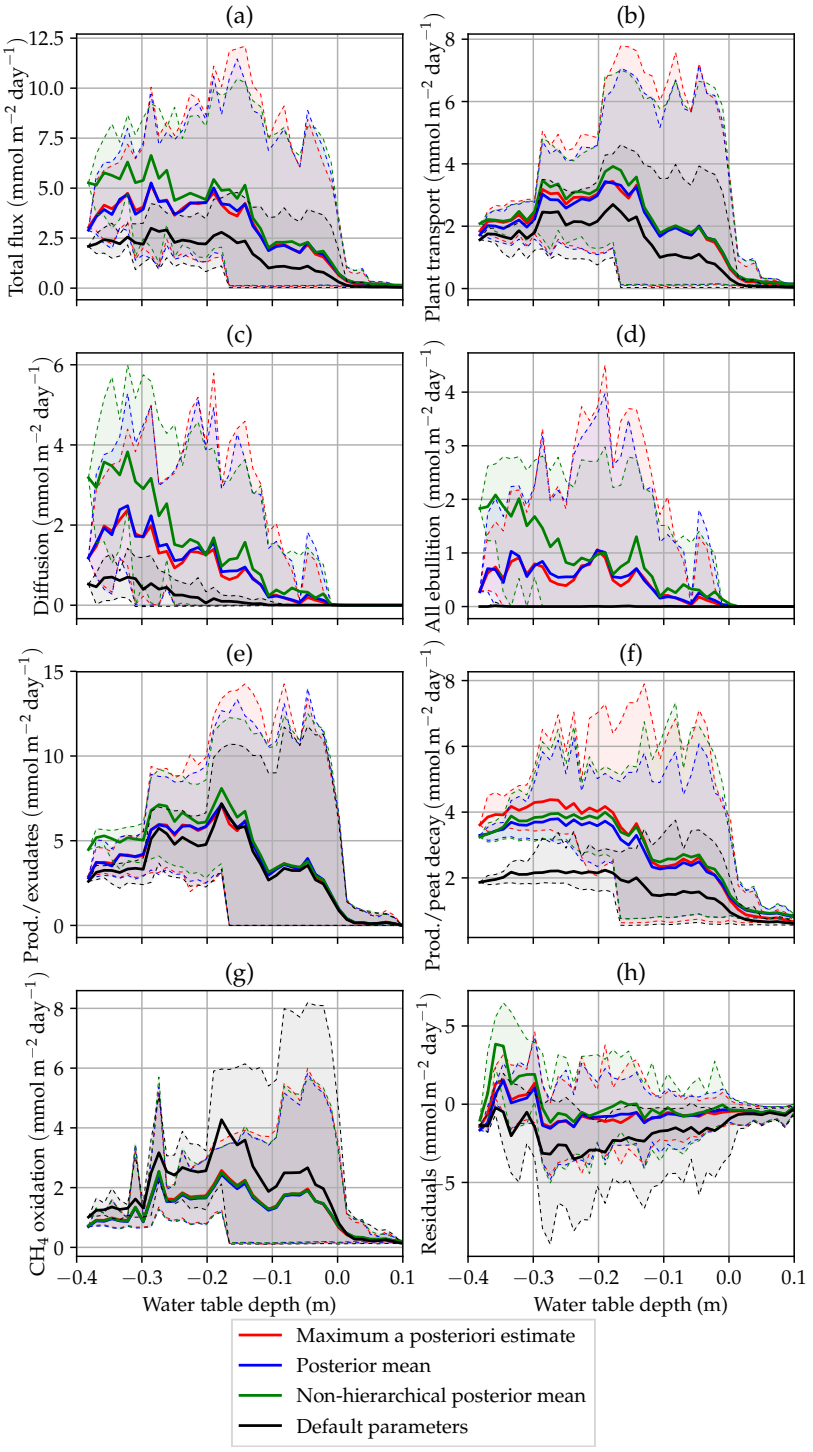

Figure 11. Means of total CH_4 emission (a), its components (b-c), total ebullition taking place (d), CH_4 production (e-f), CH_4 oxidation (g), and model residuals (h) as functions of water table depth. Shaded areas show the 5th and 95th percentiles. To look at the effect of the optimization, compare the black and the blue/red lines.

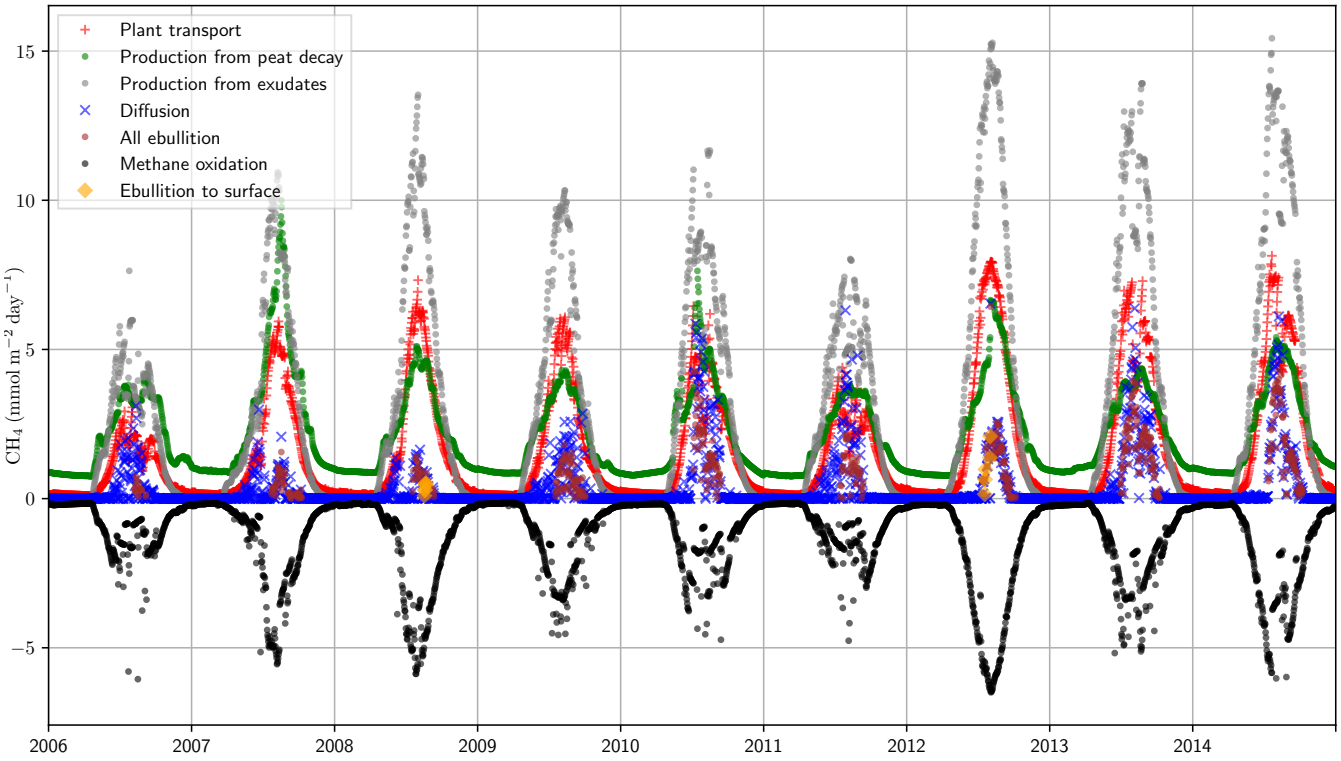

Figure 12. Diffusion, plant transport, ebullition, CH_4 production, and CH_4 oxidation time series for parameter values from the posterior mean estimate. The figure shows how only a minor part of ebullition in the end comes to the surface as ebullition. The total flux and the observations are shown in Fig. 9.

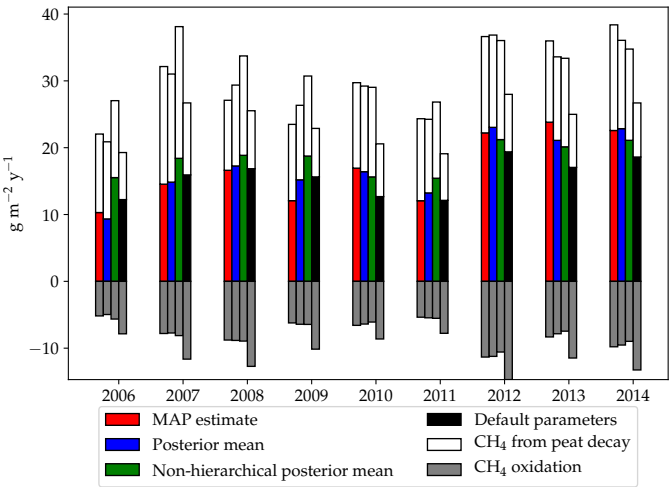

Figure 13. Annual CH_4 production in grams per square meter from root exudates (colored part) and peat decomposition (white part) for the different years. Oxidized CH_4 is shown as gray and negative.

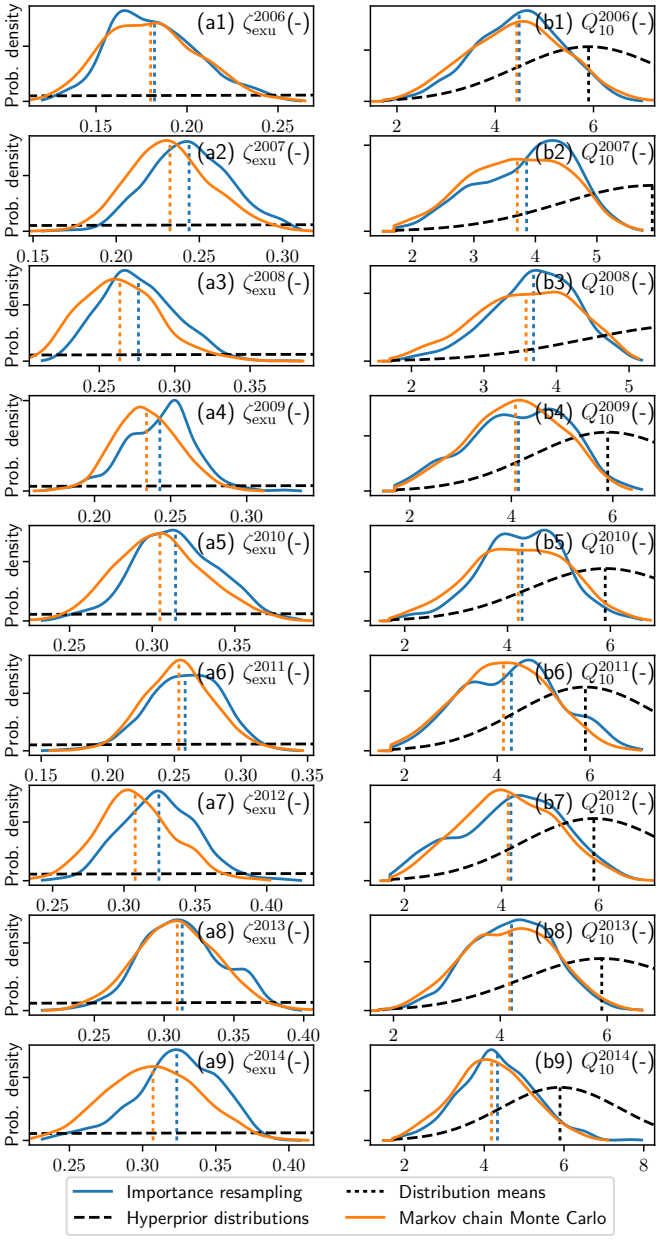

Figure 14. Posterior marginal distributions of the hierarchical parameters from both MCMC and importance sampling, along with the hyperpriors. The (a-) sub-figures are for the parameters ζ, and the (b-) sub-figures for Q_{10}. The curves shown are smoothed slightly using Gaussian kernel estimates for readability. To make these figures, 70% from the start of the MCMC chain was discarded as warm-up. The dotted vertical lines show the default parameter values and the mean values of the posterior distributions. Importance resampling had the tendency of moving the posteriors of the ζ-parameters slightly higher, despite the weaker prior used for that step.

Table 5. p and r^2 values of the regressions of the Q_{10} (-) parameters against the mean soil temperature of the 10 first weeks of the year at the depth of 35 cm, and the ζ_{exu} parameters against the sum of the net primary production of the first 130 days of the year.

$p_{Q_{10}}$	$r^2_{Q_{10}}$	$p_{\zeta_{\mathrm{exu}}}$	$r^2_{\zeta_{\mathrm{exu}}}$
0.0185	0.571	4.8e$\times$ 10^{-6}	0.957